Journal of Cleaner Production 571 (2026) 148841

Contents lists available at ScienceDirect

Journal of Cleaner Production

journal homepage: www.elsevier.com/locate/jclepro

Thermal selection of microbial consortia modulates copper corrosion toward mineral stabilization

Elena Cazzulani [a], Giorgia Ghiara [b,*], Gabriella Caucia [c], Andrea Franzetti [c], Marcella Balordi [d], Paolo Fedeli [d], Francesco Pini [d], Pierangela Cristiani [d,**], Gian Luca Chiarello [a,***]

[a] Department of Chemistry, Università degli Studi di Milano, Via Camillo Golgi 19, Milano, 20133, Italy
[b] Department of Applied Science and Technology, Politecnico di Torino, Corso Duca degli Abruzzi 24, Torino, 10129, Italy
[c] Department of Earth and Environmental Sciences, Università degli Studi di Milano Bicocca, Piazza della Scienza 1, Milano, 20126, Italy
[d] RSE-Ricerca sul Sistema Energetico S.p.A., Via Rubattino 54, Milano, 20134, Italy

HIGHLIGHTS

- Sterile conditions cause more severe Cu corrosion than any biotic condition.
- Autoclaving selects protective thermophilic archaea over corrosive bacteria.
- Bacterial activity transiently modulates early-stage copper corrosion kinetics.
- Archaeal-dominated biofilms stabilize Cu surface via redox-controlled Cu_2O.
- Chlorides drive localized corrosion; biofilm promotes diffusion-limiting patina.

GRAPHICAL ABSTRACT

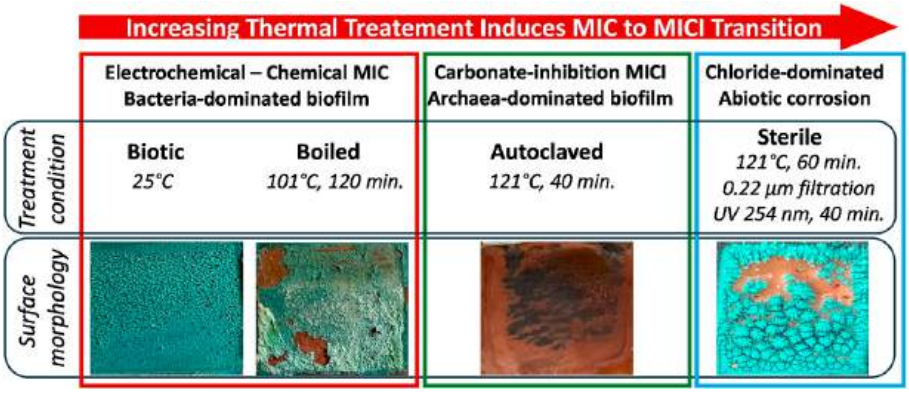

ARTICLE INFO

Keywords:
Microbiologically influenced corrosion
MIC
MICI
Copper
Microbial corrosion inhibition
Thermophiles
Archaea

ABSTRACT

Copper corrosion can be strongly modulated by microbial activity despite the intrinsic toxicity of copper ions to most microorganisms. This study investigates the corrosion behavior of high-purity copper (Cu ≥ 99.9 wt%) exposed to thermophilic bacteria and methanogenic archaea collected from a biological methanation plant. Batch experiments were conducted at 45 °C for 15 days, using the inoculum as-is (biotic), or after three distinct treatments: 1) boiling (120 min), which did not significantly alter the overall-community-level diversity and structure; 2) double autoclaving (121 °C, 20 min), which selectively enriched thermotolerant populations, and 3) sterilization, only achieved by combining autoclaving (121 °C, 60 min), filtration (Φ = 0.22 µm), and UV exposure. Microbial communities were characterized by 16S rRNA gene sequencing; corrosion was monitored by electrochemical impedance spectroscopy (EIS), scanning electron microscopy (SEM) and Raman spectroscopy. Results reveal a time-dependent transition from microbially influenced corrosion (MIC) to microbial corrosion-

* Corresponding author.
** Corresponding author.
*** Corresponding author.
E-mail addresses: giorgia.ghiara@polito.it (G. Ghiara), pierangela.cristiani@rse-web.it (P. Cristiani), gianluca.chiarello@unimi.it (G.L. Chiarello).

https://doi.org/10.1016/j.jclepro.2026.148841
Received 23 January 2026; Received in revised form 30 May 2026; Accepted 21 June 2026
Available online 24 June 2026

inhibition (MICI). Bacterial-dominated communities transiently perturbed interfacial electrochemistry and delayed passivation but did not produce the highest cumulative copper dissolution (3,1, 3,73, 3,09 mg L^{-1}, for biotic, boiled, and autoclaved inoculum, respectively). Two distinct MICI pathways were identified: Cu_2O barrier stabilization under archaeal-dominated inoculum (autoclaved), and diffusion resistance through porous phosphates precipitation in mixed bacterial-archaeal communities (biotic, boiled inoculum). Sterile conditions exhibited uninhibited chloride-driven localized corrosion and the highest copper release (7.1 mg L^{-1}). Overall, the microbial community exerts a net moderating influence on copper dissolution, and thermal selection of community composition determines which MICI mechanism prevails.

1. Introduction

Sterilization in laboratory and industrial settings typically relies on autoclaving, i.e. exposing equipment and solutions to saturated steam at 121 °C for 15–30 min under pressure (around 15 psi). This protocol is widely accepted as sufficient to inactivate nearly all known pathogens, including bacteria, fungi, yeasts, and viruses, as well as most environmental microorganisms and their spores (Rutala, 2008). However, growing evidence indicates that some thermophilic and hyperthermophile microorganisms, particularly archaea and spore-forming bacteria, can survive such thermal treatments under specific conditions (Setlow, 2006; Pikuta et al., 2007; Marquis et al., 1994; White, 1984; Cazzulani et al., 2025). These resilient organisms are frequently associated with extreme natural environments, including deep marine sediments, hydrothermal vents, and subsea ecosystems, where elevated temperatures, limited oxygen availability, and high metal concentration prevail.

Microorganisms adapted to such environments are not only capable of surviving thermal stresses, but can also colonize and persist on metallic surfaces, including materials traditionally regarded as antimicrobial, such as copper and its alloys (Solioz et al., 2010; Harrison et al., 2007).

Their capacity to adhere, form biofilms, and remain metabolically active after thermal or chemical stress challenges the assumption that standard sterilization protocols ensure microbially inert conditions. This issue is particularly relevant for systems operating at elevated temperatures, where selective pressure may favor thermophilic and hyperthermophilic populations with unusual metabolic capabilities and enhanced tolerance to metal-induced stress.

Copper and copper-based alloys are extensively used in industrial and marine-related infrastructures due to their excellent thermal conductivity, corrosion resistance, and well-documented antimicrobial properties (Yu et al., 2024). In marine environments, copper alloys are employed in heat exchangers, piping, desalination units, and antifouling applications, where they are continuously exposed to saline waters, chloride ions, and complex microbial communities. Similarly, in industrial systems such as anaerobic digesters, biological methanation reactors, and heat recovery units, copper components are frequently operated under thermophilic conditions (typically 50-65 °C), often in chemically aggressive and anaerobic environments (Cheng et al., 2024; Papirio et al., 2013). While copper's antimicrobial activity is generally considered beneficial for limiting biofouling, prolonged exposure to complex microbial consortia, especially those adapted to high temperature and redox extremes, may instead promote the selection of metal-tolerant microorganisms capable of interacting with and degrading copper surfaces (Cazzulani et al., 2026; Díaz et al., 2006; Little and Lee, 2014; Little et al., 2020).

From a mechanistic standpoint, copper corrosion is a thermodynamically driven electrochemical process involving anodic metal dissolution and cathodic reduction reactions (Little and Lee, 2014; Tait, 2018). Copper oxidation produces cuprous (Cu^+) and/or cupric (Cu^{2+}) ions, which may subsequently react with environmental anions such as chlorides, carbonates, hydroxides, or sulfides to form a variety of corrosion products, including cuprite (Cu_2O), tenorite (CuO), copper chlorides, sulfides, and mixed secondary phases (Lytle and Nadagouda, 2010). Chloride ions, which are ubiquitous in marine systems, are particularly aggressive toward copper, as they destabilize passive surface films and promote localized corrosion phenomena such as pitting (Itzhak et al., 1981).

Pitting corrosion is characterized by the formation of small, highly anodic sites that lead to accelerated and localized metal dissolution, often resulting in severe structural degradation despite limited overall mass loss. The corrosion behavior of copper becomes significantly more complex in the presence of microorganisms. Numerous studies have demonstrated that microbial activity can either accelerate or inhibit corrosion processes, depending on the nature of the microbial community, its metabolic pathways, and the physicochemical conditions at the metal–biofilm interface (Mansfeld, 2007; Videla, 2018; Garcia et al., 2012). Many environments of industrial relevance (e.g., natural waters (Amendola and Acharjee, 2022), marine cooling systems (Cristiani and Perboni, 2014), biogas digesters (Kouakou et al., 2024), deep ground (Lee et al., 2025)) support biofilm growth on copper alloys, and these biofilms can profoundly affect corrosion processes (Cristiani and Perboni, 2014), hence this phenomenon is broadly termed microbially influenced corrosion (also known as microbial corrosion, or biocorrosion). Microorganisms can accelerate corrosion of copper by different mechanisms, including: i) the production of corrosive anions (e.g., sulfides from anaerobic sulfate reducing bacteria (Li et al., 2018; Chen et al., 2014)), ii) the release of acidic metabolites (typically organic acids such as acetate (Singh and Singh, 1995)), iii) the secretion of electroactive compounds and enzymes (such as phenazines from aerobic *Pseudomonas* species (Ghiara et al., 2022)). Through different metabolic pathways, microorganisms can drastically modify the environmental conditions at the biofilm–metal interface, leading to: i) alterations in local pH, redox potential, or oxygen concentration gradients; ii) facilitation of cathodic depolarization; and iii) complexation of dissolved metal ions within extracellular polymeric substances (EPS), thereby shifting thermodynamic equilibria (Cazzulani et al., 2025; Ghiara et al., 2019, 2022; Cristiani et al., 2025). These processes can induce sharp gradients in pH, redox potential, and chemical composition within biofilms, profoundly affecting corrosion kinetics and mechanisms.

Recent advances have further highlighted the role of extracellular electron transfer (EET) as a key mechanism through which electroactive microorganisms interact with metal surfaces. In mixed-species biofilms, interspecies electron transfer, both mediated (MIET) and direct (DIET), can create synergistic electrochemical interactions that amplify or modulate corrosion beyond what individual species can achieve in isolation (Arroussi et al., 2025a). At the single-species level, model organisms such as the facultative anaerobic *Shewanella oneidensis* MR-1 have provided mechanistic insights into EET-MIC processes: depending on medium composition, electron donor/acceptor availability, and the passive state of the metal surface, this bacterium can promote corrosion through H_2-mediated electron transfer, flavin-based shuttle mechanisms, or direct cytochrome-mediated electron uptake, but may also inhibit corrosion under different conditions (Arroussi et al., 2025b). Indeed, microorganisms may also mitigate corrosion through mechanisms collectively referred to as MICI. Protective biofilms can act as diffusion barriers, consume oxidants, promote the precipitation of passivating compounds, or stabilize surface films through extracellular polymeric substances (Little and Lee, 2014; Ghiara et al., 2018). For example, strains of *Shewanella spp*. have been reported to mitigate

corrosion in specific alloy-systems, including Al 2024, brass, and mild steel exposed to artificial seawater (ASW) (Nagiub and Mansfeld, 2002). Although Al 2024 is highly susceptible to chloride induced pitting in marine and chloride containing environments, several studies have shown that specific microbial consortia, or even single Shewanella strains, can reduce pit initiation or growth under ASW test conditions, presumably through biofilm mediated modification of interfacial chemistry and/or reductive transformation of surface films (Mansfeld et al., 2002a, 2002b; Örnek et al., 2002).

The dual nature of copper in microbial environments, acting both as a target for corrosion and as a potent antimicrobial agent, has led to the development of copper-bearing (Cu-bearing) alloys designed to mitigate MIC. Recent studies on titanium-based alloys, such as Ti-6Al-4V-5Cu and cp-Ti-5Cu, have demonstrated that the integration of copper into the metal matrix can significantly inhibit the formation of biofilms by marine pathogens like *Pseudomonas aeruginosa* and *Bacillus vietnamensis* (Arroussi et al., 2022, 2023). In these systems, the continuous release of Cu^{2+} ions and the presence of specific intermetallic phases (e.g., Ti_2Cu) not only reduce bacterial attachment but also promote the stability and 'self-healing' capacity of the passive film. This suggests that when copper is structurally integrated, it can shift the balance toward MICI, reinforcing the material's surface integrity even in aggressive biotic media.

These findings highlight that the role of microorganisms in corrosion is not unidirectional, but highly dependent on microbial composition and environmental context.

Importantly, many of the microorganisms implicated in MIC and MICI in marine environments, particularly in deep-sea and hydrothermal settings, are thermophilic or hyperthermophilic archaea and bacteria, including hydrogenotrophic and methanogenic species. These microorganisms thrive under conditions of elevated temperature, high pressure, limited oxygen availability, and elevated metal concentrations, conditions that closely resemble those encountered in certain industrial biotechnological systems. Biological methanation plants, for instance, host dense consortia of hydrogenotrophic bacteria and methanogenic archaea and are frequently operated under thermophilic conditions, with periodic thermal treatments applied to enhance performance or control contamination (Bougrier et al., 2008; Gagliano et al., 2015).

In this context, the present study investigates copper corrosion in the presence of a microbial consortium that is ecologically and physiologically relevant to thermal environments common in biotechnological plants, and more simply available, rather than inoculum from deep sea hydrothermal vents. The inoculum, derived from the blowdown water of a biological methanation pilot plant, contains thermophilic and hyperthermophilic microorganisms that share key metabolic traits with microbes inhabiting hydrothermal vents and subseafloor marine systems. By subjecting this inoculum to different thermal treatments prior to copper exposure, the study explores how shifts in microbial community structure, rather than complete sterilization, affect corrosion behavior, biofilm formation, and corrosion product evolution.

Therefore, this work provides mechanistic insights into copper-microbe interactions under high-temperature, anaerobic, and chloride-containing conditions that are directly relevant to marine corrosion science, particularly in the context of deep-sea and extreme marine environments. Understanding how thermophilic microbial consortia influence copper corrosion contributes to a broader framework for predicting material performance in both advanced industrial systems and emerging marine applications operating beyond mesophilic conditions.

2. Methodology

2.1. Material preparation

Four coupons of pure copper (Cu, ≥99.9 wt%) with an area of 8.4 cm^2 were cut from a commercially available ingot (Alfa Aesar) and were used as the working electrode (WE) in this experiment. The surface of each working electrode was prepared by polishing with a lapping machine using abrasive SiC papers of different grit sizes (from 600, to 2500-grit). The polished samples were then coated with a non-conductive polymeric resin leaving exposed to the inoculum solution a precise area of 1.2 cm^2. The metal samples were electronically connected with insulated copper wires for electrochemical measurements. In addition, to ensure complete cleaning of the metal surface, copper coupons were rinsed with distilled water, degreased with ethanol (70% v/v), and subsequently exposed to UV light (254 nm) for 40 min under a sterile hood.

2.2. Microorganism pool

The pool, rich in hydrogenotrophic methanogens and bacteria, was isolated from a biological methanation pilot plant sludge operating at RSE in Milan (Italy). Microbial composition was characterized by Illumina sequencing following the procedure described in Section 3.7. Ion chromatography (IC) and inductively coupled plasma-atomic emission spectroscopy (ICP-AES) analysis of the pool are presented in Tables 6 and 7. Conductivity and pH of the bacterial pool were measured with a conductivity cell (AMEL 134) and a pH meter (AMEL 334-B) were 4.04 ms cm^{-1} and 6.96, respectively. The culture solution used in this work contained the following nutrients: $Na_2HPO_4{\cdot}12H_2O$ (896 mg L^{-1}); NH_4Cl (424 mg L^{-1}); KH_2PO_4 (216 mg L^{-1}); $MgCl_2{\cdot}6H_2O$ (80 mg L^{-1}); $CaCl_2{\cdot}2H_2O$ (60 mg L^{-1}); $FeCl_2{\cdot}4H_2O$ (16 mg L^{-1}); $CoCl_2{\cdot}6H_2O$ (6.7 mg L^{-1}); $MnCl_2{\cdot}4H_2O$ (3.3 mg L^{-1}); $NiCl_2{\cdot}6H_2O$ (0.7 mg L^{-1}); H_3BO_3 (0.3 mg L^{-1}); $ZnCl_2$ (0.3 mg L^{-1}); Na_2SeO_3 (0.3 mg L^{-1}); $CuCl_2$ (0.2 mg L^{-1}); $Na_2MoO_4{\cdot}2H_2O$ (0.1 mg L^{-1}). The phosphate system (Na_2HPO_4/KH_2PO_4) provides buffering capacity to maintain pH stability during microbial metabolic activity, as employed in operational methanation facilities. Since the inoculum was collected from a methanation plant operating with this nutrient composition, the microbial consortium was pre-adapted to these phosphate-rich, buffered conditions. CO_2, dosed as described in Section 2.3, served as the primary carbon source for autotrophic and mixotrophic members of the community, consistent with methanation process requirements.

Different thermal treatments were applied to the microbial pool before the starting of the test and subsequently tested for corrosion behavior (Table 1): i) boiling for 120 min (boiled); ii) autoclaving twice at 121 °C for 20 min (autoclaved); and iii) autoclaving at 121 °C for 60 min followed by filtration through a 0.22 μm membrane and UV-treatment at 254 nm for 40 min (sterile control). These treatments were compared with the untreated biotic solution.

2.3. Experimental set-up

For each experimental condition (biotic, boiled, autoclaved, and sterile, Table 1), tests were conducted in individual 250 mL glass electrochemical cells. Each cell was filled with approximately 200 mL of biogas-derived inoculum, either untreated (biotic) or thermally treated (boiled or autoclaved) depending on the experimental condition and hermetically sealed with a rubber stopper equipped with gas inlet and outlet lines. Electrochemical measurements were carried out using a

Table 1
Overview of the different thermal treatments applied to the inoculum, sourced from a biomethanation plant, prior to the start of the test. Each thermal treatment represents a tested condition in which the copper coupon was immersed for 15 days.

Condition	Treatement
Biotic	none
Boiled	101 °C, 120 min
Autoclaved	121 °C, 20 min, 2 cycles
Sterile	121 °C, 60 min + Filtration 0.22 μm + UV 254 nm, 40 min

three-electrode configuration consisting of a copper coupon as the working electrode (WE), a saturated KCl Ag/AgCl reference electrode (RE; E = +0.197 V vs. SHE; AMEL Srl, model 373/12), and a DSA® counter electrode (CE). The RE was positioned near the WE, thus minimizing solution resistance and eliminating the need for IR compensation.

All experiments were performed at 45 °C, a good compromise between mesophilic and thermophilic conditions that is representative of operational conditions in biological methanation plants (Pincam et al., 2026), in a thermostatically controlled sand bath. Microaerophilic conditions were established by initial CO_2 sparging for 30 min (44.5 mmol injected into the headspace/solution during the 30-min sparging step). CO_2 sparging, although not standard for deoxygenation, was deliberately used to maintain microaerophilic conditions consistent with methanation process requirements, the source inoculum and to supply inorganic carbon for hydrogenotrophic methanogenesis (Luo and Angelidaki, 2012; Bassani et al., 2015). The temperature remained stable throughout the entire testing period. Four different treatments of the inoculum were investigated, as described in Section 3.2.

Prior to use, all glassware was washed with sodium hypochlorite, sterilized in an oven at 121 °C, and subsequently rinsed with 70% (v/v) ethanol. To prevent environmental contamination, the entire experimental setup was sterilized under a vertical laminar-flow UV hood (254 nm, 45 min). Sample preparation was also conducted under the same sterile conditions. All tests were performed in duplicate to ensure reproducibility of the electrochemical response of copper coupons exposed to the differently treated inocula. Indeed, for each condition (Table 1), four brass coupons were tested simultaneously under identical conditions. Two coupons were dedicated to electrochemical measurements throughout the 15-day exposure period. The other two coupons were used for post-test characterization: one coupon was used for surface characterization without altering the corrosion products morphology, while the other was used for both molecular analyses and surface characterization after biofilm removal from a defined area (0.7 cm^2) of the exposed surface (1.2 cm^2). The progression of MIC was monitored over a 15-day exposure period.

2.4. Electrochemical measurements

Electrochemical analyses were conducted in duplicate using a Gamry potentiostat/galvanostat (Interface 1000) in a conventional three-electrode cell configuration. The open circuit potential (OCP) was continuously monitored over the 15-day exposure period for all experimental conditions (biotic, boiled, autoclaved, and sterile).

Linear polarization resistance (LPR) measurements were performed after 1 and 15 days of exposure. Polarization curves were recorded by scanning the potential from −0.020 V to +0.020 V versus the OCP at a scan rate of 0.167 mV s^{-1}. The polarization resistance (*Rp*) was determined from the potential-current curve by linear regression analysis.

Electrochemical impedance spectroscopy measurements were carried out using a sinusoidal perturbation of ±10 mV versus OCP over a frequency range from 100 kHz to 0.01 Hz, with a resolution of 10 points per decade. Impedance spectra were collected after 1, 7, and 15 days of testing. All electrochemical data were normalized to the exposed surface area of the samples (1.2 cm^2). For each condition, the most representative datasets were selected and discussed.

2.5. Surface analysis

Corrosion tests were performed in duplicate to enable both morphological characterization of corrosion products and compositional analysis of the associated biofilm. One coupon was reserved exclusively for surface characterization in order to preserve the morphology of the corrosion products. The second replicate was used for molecular analyses as well as for biofilm surface characterization. In this case, the biofilm was mechanically removed from a defined area (0.7 cm^2) of the exposed coupon surface (total exposed area: 1.2 cm^2). The remaining surface was subsequently dried in an oven at 100 °C for 15 min under air atmosphere to allow surface characterization of the residual biofilm.

Morphological observations and chemical characterization of corrosion products were carried out on both the surface and cross sections of the coupons. Post-exposure surface analyses were performed using: i) a light optical microscope (Nikon Eclipse MA2000); and ii) a scanning electron microscope (JEOL JSM-IT500 LV) equipped with secondary electron (SE) and backscattered electron (BSE) detectors. SEM observations were conducted at an accelerating voltage of 20 kV and a beam current of 65 μA. Elemental composition was determined by Energy-Dispersive X-ray Spectroscopy (EDS). Quantitative analysis was performed using the ZAF correction implemented in the JEOL software suite, providing reliable results for elements with atomic number ≥11. Lighter elements (e.g., oxygen) and concentrations below 0.3 wt% were considered semi-quantitative and reported only when clearly identifiable peaks were observed in the spectra.

Raman spectroscopy analyses were conducted using a Horiba XploRA PLUS system coupled with an Olympus BX43 microscope and a long-working-distance 50× objective (NA = 0.50). Spectra were collected using a 532 nm solid-state laser and a 2400 lines/mm diffraction grating. The combination of these settings with the air-cooled Peltier CCD detector (1024 × 256 pixels, pixel size 26 × 26 μm^2) ensured a spectral resolution of approximately 1 cm^{-1}. To prevent laser-induced alteration of the corrosion products, neutral density filters were applied to reduce the laser power from 25% to 1%. All spectra were acquired over the range 100–2000 cm^{-1}.

Cross sections were prepared to evaluate the spatial distribution of corrosion products and to assess the possible presence of biofilm at the metal surface. Samples were mounted in cold-curing epoxy resin and mechanically polished using silicon carbide (SiC) papers up to 1200 grit, followed by final polishing with diamond paste down to 1 μm. Sample preparation was performed in accordance with the ASTM E3–01 standard procedure.

2.6. Solution analysis

Chemical analyses of the test solutions were performed at both the beginning and the end of the experiments for each condition (biotic, boiled, autoclaved, and sterile control) to quantify the release of the main alloying elements and to monitor changes in the concentration of selected anionic species (carbonates, acetates, formates, and oxalates). The concentrations of Cu, Zn, S, and P ions were determined by inductively coupled plasma-atomic emission spectroscopy (Analytik Jena PlasmaQuant PQ 9000), operated at a radiofrequency power of 1200 W.

Anionic species in solution were analyzed by ion chromatography (Dionex ICS 1000) equipped with an S9-SC analytical column and an AMMSIC chemical suppressor. For each analysis, a 10 mL aliquot of solution was collected using a sterile syringe and stored at 2 °C until measurement.

2.7. Molecular and bioinformatic analyses

Samples for the analysis included the biofilm collected from the electrode with sterile swabs, the solution and the original inoculum, obtained by using a 10 mL syringe. Samples were stored at −20 °C until analysis. DNA was extracted with the Fast DNA® Spin for Soil kit (MP Biomedicals, Solon, OH, USA) according to the manufacturer's instructions. To extract DNA from the swabs, they were cut with sterilized scissors directly into the MT Lysing matrix E-tube of the kit. Liquid samples instead were filtered on nitrocellulose filters with a pore size of 0.22 μm and DNA was subsequently extracted from half of the filters. DNA quality was assessed through a first PCR on the extracted DNA and on its dilutions 1:10 and 1:100. Sequencing was performed by MiSeq Illumina (Illumina, Inc., San Diego, CA, USA) on the 16S rRNA gene of

both bacteria and archaea. For bacteria, a first PCR was performed on the V5-V6 hypervariable region of the 16S rRNA gene with the primers 783F (5′-CAGGATTAGATACCC-3′) and 1027R (5′-CGACRRCCATGCAN-CACCT-3′) modified with homemade barcodes and Illumina adapters. For each sample, 2 × 50 μL volume PCR reactions were prepared with 25 μL of GoTaq G2 Green Master Mix (Promega Corporation, Madison, WI, USA), 12.5 μL of MilliQ water, 2.5 μL of DNA and 1 μM of each primer. The PCR cycling conditions included an initial denaturation at 94 °C for 5 min, followed by 27 cycles at 94 °C for 50 s, 47 °C for 30 s, 72 °C for 30 s, and a final extension at 72 °C for 5 min. For archaea, primers 349F (5′-GYGCASCAGKCGMGAAW-3′) and 571R (5′-GCTACGGNYSCTTTARGC-3′) modified with homemade barcodes and Illumina adapters were chosen to amplify the V4 hypervariable region of the 16S rRNA. For each sample, 2 × 50 μL volume PCR reactions were performed with 0.5 μL of Phusion Plus Master Mix (ThermoFisher Scientific, Waltham, MA, USA), 19.76 μL of MilliQ water, 2.5 μL of DNA, 10 μL of GC enhancer, 10 μL of Buffer containing 1.7 mM of $MgCl_2$, 1 μL of dNTPs (0,2 mM) and 0.5 μM of each primer. The PCR cycling conditions included an initial denaturation at 98 °C for 30 s, followed by 32 cycles at 98 °C for 10 s, 60 °C for 10 s, 72 °C for 30 s and a final extension at 72 °C for 5 min. Amplicons were then purified using the Wizard® SV Gel and PCR Clean-up System (Promega Corporation, Madison, WI) and quantified with Qubit® (Life Technologies, Carlsbad, CA). Groups of nine amplicons with 6 unique barcodes pairs were pooled to obtain a single library according to a homemade protocol. Further library preparation and sequencing were done with Illumina-MiSeq® platform (Illumina, Inc., San Diego, CA, USA) with a 300 bp × 2 paired-end protocol at the Facility of the University of Milano-Bicocca. Quality-filtered reads were assembled into Amplicon Sequence Variants (ASVs) using the dada2 pipeline (Callahan et al., 2016). Taxonomic classification of ASVs was performed with the RDP classifier (confidence >80%).

2.8. Statistical analysis

In this study, a cluster analysis was performed on the Hellinger transformed ASV dataset with the software R (version 4.3.1) with a complete method to determine the similarity between samples. Species' richness was assessed across the three different treatments (biotic, boiled and autoclaved) and for each substrate (inoculum, solution and biofilm). For each substrate, rarefaction curves were generated, using the lowest number of ASV as cutoff to ensure a correct comparison between samples.

3. Results

3.1. Open circuit potential

Fig. 1 reports the average open circuit potential (E vs Ag/AgCl sat.) of the Cu samples over a 15-day immersion period in four different conditions: untreated biomethanation solution (biotic), boiled, autoclaved and sterile control. The data reported represents the mean value of two replicates with the relative error bars representing the standard deviation. OCP measurements were evaluated at a starting pH of 6.96.

The evolution of the OCP revealed distinct trends depending on the thermal treatment applied to the microbial pool. Both the autoclaved and control samples exhibited a rapid initial increase in potential, stabilizing around −0.01 V vs Ag/AgCl. Notably, the control condition showed a marked decrease in potential after day 7, likely to indicate the breakdown or destabilization of protective surface films and a transition toward more active corrosion conditions.

In contrast, both the biotic and boiled samples exhibited a more gradual rise in potential, reaching a stable value near −0.01 V vs Ag/AgCl only after approximately 9-10 days. This slower kinetic behavior suggests a delayed establishment of surface equilibrium, possibly influenced by ongoing microbial activity or slower film formation.

The rapid shift toward a more noble potential observed in both the autoclaved and control conditions may reflect reduced corrosion activity and the formation of a relatively stable passive film on the copper surface. Conversely, the initially low and progressively increasing potentials recorded in the biotic and boiled conditions (starting at approximately −0.10 V vs Ag/AgCl) point to ongoing anodic dissolution of copper, likely driven by microbial metabolic processes and associated localized chemical changes at the metal–solution interface.

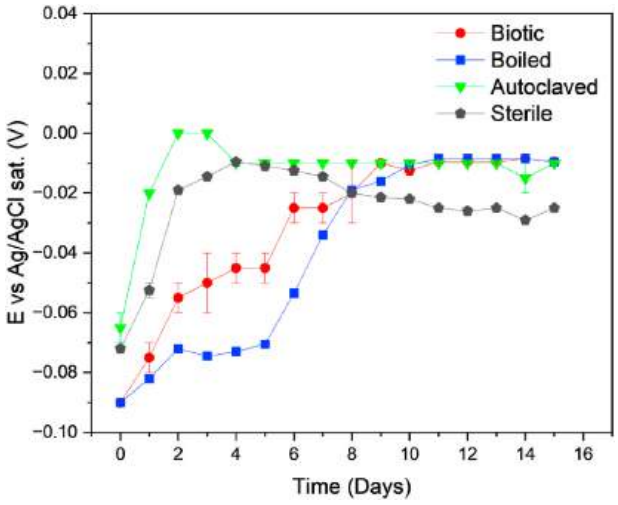

Fig. 1. Open circuit potential of Cu samples over the entire period (15 days) of the test under microaerophilic conditions. Copper samples were monitored in two differently treated inocula: boiled and autoclaved, and compared with the not treated biotic inoculum and its sterile control.

These observations indicate that the active microbial community transiently perturbs interfacial electrochemistry by sustaining more negative potential values and delaying passivation in the early exposure phase. However, this kinetic perturbation does not translate into greater cumulative copper dissolution, as demonstrated by the ICP-AES data discussed in Section 3.7. Autoclaving, by selecting for an archaeal-dominated community, favors the early development of a dense Cu_2O protective film, consistent with the highest polarization resistance values recorded across all conditions.

3.2. Linear polarization resistance

Polarization curves were carried out for each condition only on day 1 and day 15 of exposure to minimize disturbance of the interface during the test. LPR was estimated by performing a linear interpolation of the current (*I*) versus potential (*E*) curve, in the linear range of the curve around the corrosion potential of 20 mV) (Jankowski and Juchniewicz, 1980), which is related to the corrosion rate using the Stern-Geary equation, but with relevant limitations in case of localized corrosion or pitting (Perez, 2016). The results of the LPR measurements are summarized in Table 2.

As data show, all experimental conditions exhibited a decrease in polarization resistance over time. On day 1, thermally treated conditions (boiled, autoclaved and sterile) showed higher *Rp* values compared to the biotic condition, suggesting that the absence or reduction of active

Table 2
Linear polarization resistance results (mean ± standard deviation) measured after 1 and 15 days of exposure for each considered condition (biotic, boiled, autoclaved and sterile).

Time days	Biotic kΩ • cm^2	Boiled kΩ • cm^2	Autoclaved kΩ • cm^2	Sterile kΩ • cm^2
1	0.28 ± 0.073	0.73 ± 0.21	1.2 ± 0.47	0.38 ± 0.26
15	0.20 ± 0.057	0.13 ± 0.034	0.35 ± 0.067	0.11 ± 0.036

microbial populations initially facilitate a more robust passivation response. The autoclaved condition consistently displayed the highest *Rp* values (1.20 and 0.35 kΩ cm^2) throughout the experiment, indicating the greatest overall corrosion resistance among all tested conditions.

The biotic condition showed the lowest polarization resistance from the outset, consistent with microbially mediated perturbation of the interfacial electrochemistry and a delay in passive film formation. It is important to note, however, that lower *Rp* values reflect the kinetics of interfacial processes and do not directly translate into greater cumulative copper dissolution.

Interestingly, the sterile condition did not show high resistance values, indicating that MIC is not the sole corrosion phenomenon occurring on the copper surface. On Day 1, the sterile condition yielded an *Rp* of 0.38 ± 0.26 kΩ cm^2, approximately half the value recorded for the boiled condition (0.73 ± 0.21 kΩ cm^2). Although the standard deviations partially overlap, this nearly twofold difference in mean values is electrochemically significant, as it suggests that the microbial population present in the boiled condition does not significantly affect the formation of a passive layer on the material surface. By Day 15, the sterile control exhibited the lowest *Rp* value (0.11 kΩ cm^2), falling below even the biotic condition (0.20 kΩ cm^2). This reversal suggests that abiotic chloride-driven corrosion processes, uninhibited by any microbial or biofilm-mediated stabilization, dominate the long-term corrosion behavior under sterile conditions affecting the passive film.

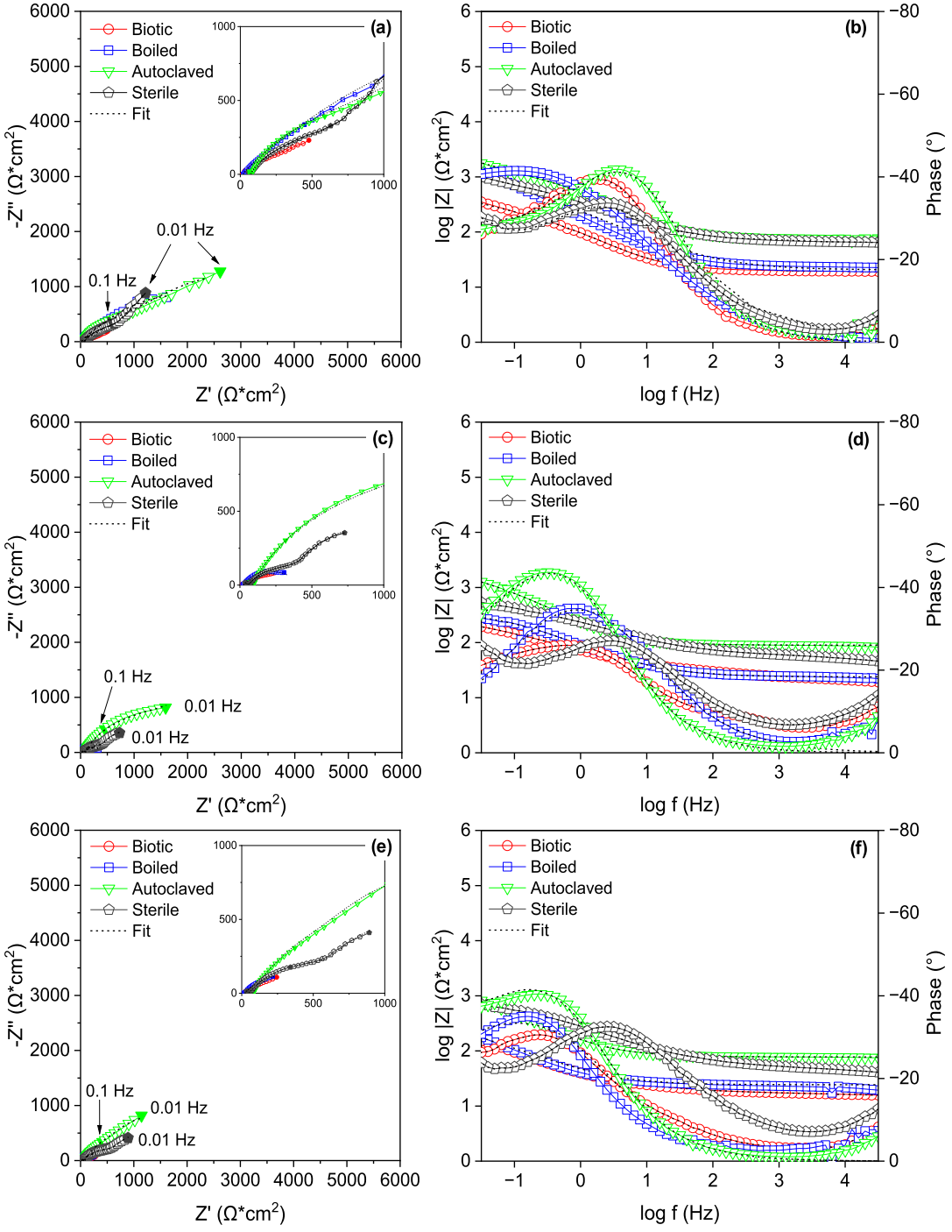

Fig. 2. Nyquist and Bode plots of Cu tested in the biotic, boiled, autoclaved and sterile inocula under microaerophilic conditions after a-b) 1 day, c-d) 7 days and e-f) 15 days.

It is important to note that the LPR technique provides an average assessment of the electrochemical behavior normalized to the entire exposed surface, which does not represent phenomena such as the initiation of pitting corrosion, which is characteristic of pure copper (Vivier and Orazem, 2022). Therefore, a careful interpretation of the *Rp* value is essential in the light of this limitation.

3.3. Electrochemical impedance spectroscopy

Electrochemical impedance spectroscopy was used to investigate more in deep interfacial processes at the electrode-solution boundary, including capacitive phenomena, charge transfer and mass transport, which greatly influence kinetics of electrochemical reactions, determining the capacitive (*C*) and resistive (*R*) behavior of the system. EIS measurements were carried out with 10 points per decade, in the frequency range of 100 kHz-0.01 Hz, at different exposure times: after 1, 7, and 15 days. The results of the impedance measurements are presented as both Bode and Nyquist plots (Fig. 2), showing the real (Z') and imaginary (Z'') components of the impedance, as well as the impedance modulus ($log\,|Z|$) and phase angle as a function of frequency (log f). The shape of the impedance curves varies noticeably among the different systems, with each condition showing a distinct and progressively evolving profile. During the first week of exposure, nearly all conditions exhibit a primary semicircle in the Nyquist plot, slightly depressed toward the x-axis, an indication of non-ideal capacitive behavior and interfacial dispersion at the metal–solution boundary (Moradi et al., 2022). The presence of a secondary semicircle can also be discerned. This suggests heterogeneity in surface reactivity, likely due to variations at the interface and in surface film properties. At 7 days, the sterile condition presents a secondary, broader semicircle appearing at very low frequencies. This feature implies the presence of at least two distinct electrochemical processes occurring simultaneously at the interface, possibly related to separate resistive or capacitive contributions from surface films and charge transfer. After 15 days of exposure, the impedance spectra for all conditions (except for the control) begins to show a shift in the low-frequency region toward a linear response with a slope approaching 45°. This change is characteristic of Warburg (*W*) impedance and suggests that diffusion-controlled processes, such as ion transport through corrosion products or biofilms, have become more prominent over time.

In terms of magnitude, the autoclaved system consistently exhibits the highest overall impedance response across all time points, surpassing those of the biotic, boiled, and sterile conditions. This suggests that the autoclaved environment promotes the formation of a more resistive interfacial layer, possibly due to the absence of aggressive microbial activity on the surface. It is important to emphasize that, in cases of significant corrosion, the capacitive contribution of the biofilm formed on the surface during the test is generally negligible, as it is masked by the more dominant contributions from corrosion products (Brug et al., 1984; Medeiros et al., 2018).

3.4. Equivalent circuit analysis

The impedance data were systematically post-processed fitting the experimental results by the equivalent electrical circuit (EEC) models (I-III) shown in Fig. 3. The choice of appropriate equivalent electrical circuits (EECs) for each condition was guided by the physicochemical processes occurring at the copper/solution interface, in accordance with established principles of impedance interpretation (causality, linearity, and stability) (Orazem and Tribollet, 2008). Distinct EECs were necessary because microbial selection induced by thermal treatment led to fundamentally different corrosion mechanisms and surface film structures, as confirmed by cross-sectional SEM–EDS analysis (See Section 3.3). Each circuit element was assigned on the basis of characteristic frequency domains and impedance magnitudes. The validity of constant phase element assignments was further assessed using Brug's equation (Brug et al., 1984), ensuring that the resulting effective capacitance (*Ceff*) values were consistent with either double-layer or film capacitance. Finally, these assignments were corroborated by surface analyses indicating the presence or absence of protective layers (See Section 3.3).

The temporal evolution of the EECs (e.g., in the biotic condition, where three different circuits were required on days 1, 7, and 15) reflects real mechanistic changes in the corrosion process, rather than arbitrary model selection. Indeed, circuit elements corresponding to specific physical or interfacial processes were identified, including solution (*Rs*), charge transfer resistances (*Rct*), double-layer (*CPEdl*) and film electrical properties (*Rf* and *CPEf*), and *W* impedance components (coefficient of determination $\chi^2 = 10^{-4}$). Ideal capacitive behavior was not observed, as experimental data in all systems deviated from that of a pure capacitor. Instead, the capacitive contribution was modeled using a constant phase element (*CPE*), which accounts for the non-ideal, frequency-dependent behavior commonly encountered in electrochemical interfaces. The impedance of a *CPE* (*ZCPE*) is described by the expression (Eq. (1)) (Arroussi et al., 2024):

$$ZCPE = \frac{1}{Y_0(j\omega)^n} \tag{1}$$

where Y_0 is the capacitance, ω is the angular frequency ($2\pi\nu$) and *n* is dimensionless exponent that characterizes the deviation from ideal capacitive behavior. The exponent ranges from 0 to 1, where 1 corresponds to an ideal capacitor and 0 to an ideal resistor. Values between 0.5 and 1 indicate a distributed or non-ideal system, commonly associated with surface roughness, porosity, or other forms of interfacial heterogeneity.

Fitting results are summarized in Tables 3–6, along with a detailed attribution of their corresponding electrochemical parameters.

The biotic condition exhibited the most complex corrosion behavior among all tested environments. To accurately model its electrochemical response over time, three distinct EECs (I-III) on Fig. 3 were used. On day 1, the electrochemical response of the system is best described by EEC I, which captures dominant diffusive behavior. This model incorporates two-time constants, consisting of an *R//CPE* (resistor in parallel with a constant phase element) mesh, followed by a *W* element. The first time constant is associated with the *Rct* and the *Cdl* as interpreted through

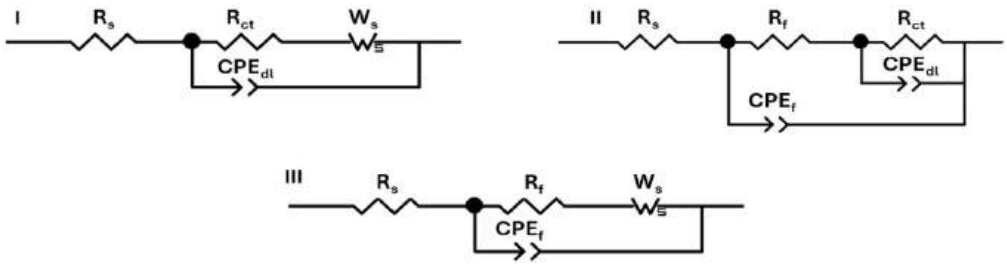

Fig. 3. Equivalent electrical circuits I – III used to model impedance data.

Table 3
Fit results using the EECs from Fig. 3 for the biotic condition. Values are expressed as mean ± standard deviation. Depending on the EEC used, parameters that are not detected are reported as 'n.d.', whereas parameters that are not applicable are indicated as 'n.a.'.

EEC	Time days	*Rs* Ω • cm^2	*Rct* kΩ • cm^2	*CPEdl Q* $k\Omega^{-1}$• cm^{-2}• s^n	*CPEdl-n*	*Rf* kΩ • cm^2	*CPEf Q* $k\Omega^{-1}$• cm^{-2}• s^n	*CPEf-n*	*W* kΩ • cm^2	*Ceff* μF • cm^{-2}	Rtot kΩ • cm^2
I	1	20 ± 2	0.170 ± 0.003	2.4 ± 0.19	0.73 ± 0.05	n.d.	n.d.	n.d.	2.7 ± 0.12	740 ± 28	2.9 ± 0.123
II	7	18 ± 2	0.086 ± 0.020	7.3 ± 2.0	0.55 ± 0.09	0.49 ± 0.03	0.48 ± 0.014	0.98 ± 0.01	n.d.	130 ± 19	0.58 ± 0.050
III	15	18 ± 5	n.d.	n.d.	n.d.	0.39 ± 0.09	0.015 ± 0.0001	0.52 ± 0.08	0.09 ± 0.006	n.a.	0.48 ± 0.096

Table 4
Fit results using the EECs from Fig. 3 for the boiled condition. Values are expressed as mean ± standard deviation. Depending on the EEC used, parameters that are not detected are reported as 'n.d.', whereas parameters that are not applicable are indicated as 'n.a.'.

EEC	Time days	*Rs* Ω • cm^2	*Rct* kΩ • cm^2	*CPEdl Q* $k\Omega^{-1}$• cm^{-2}• s^n	*CPEdl-n*	*Rf* kΩ • cm^2	*CPEf Q* $k\Omega^{-1}$• cm^{-2}• s^n	*CPEf-n*	*W* kΩ • cm^2	*Ceff* μF • cm^{-2}	*Rtot* kΩ • cm^2
II	1	20 ± 1	0.9 ± 0.043	1.3 ± 0.01	0.59 ± 0.01	2.7 ± 0.27	1.6 ± 0.06	0.59 ± 0.03	n.a	98 ± 0.01	3.6 ± 0.27
II	7	24 ± 6	0.36 ± 0.07	3.9 ± 0.19	0.61 ± 0.01	0.044 ± 0.01	0.074 ± 0.001	0.95 ± 0.02	n.a.	800 ± 69	0.41 ± 0.08
III	15	24 ± 1	n.d.	n.d.	n.d.	0.052 ± 0.005	8.5 ± 0.18	0.67 ± 0.01	0.41 ± 0.01	n.a.	0.46 ± 0.02

Table 5
Fit results using the EECs from Fig. 3 for the autoclaved condition. Values are expressed as mean ± standard deviation. Depending on the EEC used, parameters that are not detected are reported as 'n.d.', whereas parameters that are not applicable are indicated as 'n.a.'.

EEC	Time days	*Rs* Ω • cm^2	*Rct* kΩ • cm^2	*CPEdl Q* $k\Omega^{-1}$• cm^{-2}• s^n	*CPEdln*	*Rf* kΩ • cm^2	*CPEf Q* $k\Omega^{-1}$• cm^{-2}• s^n	*CPEf-n*	*W* kΩ • cm^2	*Ceff* μF • cm^{-2}	*Rtot* kΩ • cm^2
I	1	76 ± 1	0.46 ± 0.04	30 ± 1.7	0.77 ± 0.01	n.a.	n.a.	n.a.	4.29 ± 0.08	92 ± 4.5	4.8 ± 0.12
I	7	90 ± 1	1.2 ± 0.016	1.3 ± 0.01	0.72 ± 0.01	n.a.	n.a.	n.a.	5.2 ± 0.48	590 ± 32	6.4 ± 0.49
III	15	78 ± 1	n.d.	n.d.	n.d.	0.90 ± 0.01	2.4 ± 0.03	0.71 ± 0.06	1.5 ± 0.12	n.a.	2.4 ± 0.12

Table 6
Fit results using the EECs from Fig. 3 for the sterile condition. Values are expressed as mean ± standard deviation. Depending on the EEC used, parameters that are not detected are reported as 'n.d.', whereas parameters that are not applicable are indicated as 'n.a.'.

EEC	Time days	*Rs* Ω • cm^2	*Rct* kΩ • cm^2	*CPEdl Q* $k\Omega^{-1}$• cm^{-2}• s^n	*CPEdl-n*	*Rf* kΩ • cm^2	*CPEf Q* $k\Omega^{-1}$• cm^{-2}• s^n	*CPEf-n*	*W* kΩ • cm^2	*Ceff* μF • cm^{-2}	*Rtot* kΩ • cm^2
I	1	66 ± 1	0.68 ± 0.02	0.8 ± 0.02	0.61 ± 0.01	n.a	n.a	n.a	3.1 ± 0.29	110 ± 19	3.8 ± 0.29
II	7	56 ± 1	0.55 ± 0.02	1.5 ± 0.03	0.53 ± 0.01	0.85 ± 0.07	0.17 ± 0.12	0.9 ± 0.03	n.a.	150 ± 14	1.4 ± 0.09
II	15	47 ± 1	0.89 ± 0.03	1.3 ± 0.02	0.52 ± 0.01	0.89 ± 0.15	0.22 ± 0.04	0.97 ± 0.06	n.a.	97 ± 0.3	1.8 ± 0.18

Table 7
Ion chromatography analysis of acetic, formic, oxalic acids and carbonates in biotic, boiled, autoclaved inocula and sterile control. Results of the concentration (ppm) are compared before the start of the test (initial concentration) and after the 15-day of the test (final concentration).

	Biotic		Boiled		Autoclaved		Sterile	
	Concentration (mg L^{-1})[a]							
	Initial	Final	Initial	Final	Initial	Final	Initial	Final
Acetates	BDL	132.2	178.1	899.2	6.80	30.8	BDL	BDL
Formates	9.010	BDL	8.201	BDL	BDL	1.0	BDL	BDL
Oxalates	2171	2256	2086	2637	1814	2158	1207	1407
Carbonates	120.0	113.6	126.4	77.10	222.5	421.0	BDL	BDL

[a] *Concentrations below the limit of detection are indicated as "BDL" in the table.*

Brug's equation (Feng et al., 1997). This formulation allows for the calculation of the *Ceff* using the *CPE* parameters (magnitude and exponent *n*), as well as the values of *Rs* and *Rct*. Valid *Ceff* values typically fall within the range of 10^{-4} to 10^{-5} F cm^{-2}, confirming the physical consistency of the fit.

The *W* element represents the diffusion-limited transport of electroactive species at the electrode–electrolyte interface, indicating that ion migration plays a significant role in the early-stage corrosion process under biotic conditions.

At 7 days, the corrosion mechanism is best represented by EEC II of Fig. 3, which consists of two *R//CPE* (resistor in parallel with constant phase element) meshes arranged in a ladder configuration. The first time constant corresponds to the *Rct* and the *Cdl*, characterizing the electrochemical processes at the metal–electrolyte interface. The second time constant accounts for the electrical properties (the resistance *Rf* and non-ideal capacitance *CPEf*) of a surface film that has developed at the interface. Post-experimental surface analyses suggest that this film is primarily composed of copper phosphates. Although this copper

phosphate film does not constitute a classical passive layer in the electrochemical sense, as it is insufficiently stable to function as an electron-transfer barrier, it nonetheless introduces a degree of diffusion resistance that slows ionic transport between the metal surface and the bulk solution (Lizoul et al., 2024). Its role is more accurately described as one of partial, diffusion-mediated stabilization, which becomes increasingly relevant over longer exposure times (Edwards et al., 2002; Glarum and Marshall, 1985; Zhe and Pehkonen, 2004).

After 15 days of exposure, the biotic coupon once again exhibits a diffusion-controlled corrosion mechanism (Table 3), modeled by EEC III of Fig. 3. This circuit consists of an *R//CPE* mesh in series with a *W*, indicative of mass transport limitations. At this stage, the formation of a more uniform patina hinders the contribution of the charge transfer and double-layer components. As a result, the *Rf* and *CPEf* are attributed to the electrical properties of the patina itself, which, according to surface analyses, are likely to contain complex copper phosphates. The inclusion of the Warburg element reflects diffusion-limited transport of Cu ions through the patina toward the solution interface, suggesting that although the patina has developed more completely, it does not eliminate ion mobility, highlighting its porous nature.

The boiled coupon exhibits a corrosion mechanism closely resembling that observed under biotic conditions, especially at 7 and 15 days, which can be modeled with EEC II and EEC III, respectively (Fig. 3 and Table 4). On day 1, the electrochemical behavior is characterized by a less diffusion-dominated response and a signal response likely due to the early formation of a patina composed of corrosion products. Under these conditions, the system is best modeled by EEC II of Fig. 3, featuring two *R//CPE* meshes, as observed at 7 days. These elements are attributed to the *Rct* and *Cdl*, as well as the *Rf* and *CPEf*, which are most likely associated with the development of copper oxide layers. At 15 days, the same corrosion products observed on the biotic coupon are also detected on the boiled coupon.

The autoclaved condition exhibits a different behavior, with a diffusion-driven corrosion mechanism consistently throughout the entire duration of the experiment (Fig. 3 and Table 5). Indeed, electrochemical behavior is best modeled at each time point by an equivalent circuit consisting of an *R//CPE* mesh in series with a *W* element, reflecting ion transport limitations at the interface. Up to day 7, the system is most accurately described by EEC II. In this configuration, the first-time constant is attributed to the *Rct* and *Cdl*, suggesting the formation of a non-uniform patina, primarily composed of copper oxides and possibly hydroxides. By day 15 (EEC III), the patina appears to have become more compact and uniformly distributed across the surface, effectively masking the contributions of *Rct* and *Cdl*. As a result, the *R//CPE* mesh at this stage is mostly determined by the protective electrical properties of the film itself (*Rf* and *CPEf*), rather than charge transfer processes.

The sterile coupon exhibits distinctive behavior. On day 1, its corrosion response closely mirrors that observed under biotic and autoclaved conditions and is best represented by EEC I (Table 6 and Fig. 3). At this initial stage, the mechanism is diffusion-controlled, characterized by *Rct* and *Cdl* in series with a *W* element, which reflects ionic transport limitations at the metal–electrolyte interface. Between days 7 and 15, the corrosion mechanism evolves and is more accurately described by EEC II, comprising two R//CPE meshes. The first time constant represents interfacial electrochemical reactions (*Rct//Cdl*), while the second corresponds to the development of a surface film (*Rf//CPEf*). Post-experiment analyses (see following section) reveal a nonhomogeneous stratified film structure: an inner layer of copper oxides and an outer layer likely composed of copper chlorides and oxychlorides. This layered configuration indicates a progressive transformation and accumulation of corrosion products over time, resulting in increased heterogeneity in surface chemistry and electrochemical behavior.

The evolution of the logarithmic resistance contributions for each condition through time is represented in Fig. 4.

The *Rtot* obtained from the electrochemical impedance spectroscopy measurements corroborate the corrosion trends observed via the linear polarization resistance technique. Throughout the experiment, both the boiled and biotic conditions exhibit the lowest corrosion resistances, reflecting more severe corrosion behavior. By the end of the test, their total resistance values are approximately one order of magnitude lower than those measured in the autoclaved and sterile conditions ($\sim 10^2$ vs. $\sim 10^3\ \Omega\ cm^2$), likely due to the persistent influence of microbial activity. This divergence in corrosion resistance becomes especially pronounced from day 7 onward, highlighting the increasing impact of biological factors over time. Notably, the *Rf* plays a dominant role in determining *Rtot* and aligns well with the observations previously described. An interesting contrast emerges when examining the *Rct*, which follows opposing trends depending on the exposure condition. In the sterile and autoclaved environments, *Rct* increases over time, while a sharp decline is visible in the biotic and boiled conditions, suggesting that microbial activity facilitates electron transfer, likely through the production of redox mediators that accelerate the electrochemical corrosion process.

3.5. Surface characterization

Fig. 5 shows the macroscopic variation on the Cu surfaces after 15-days of tests in biotic, boiled, autoclaved and sterilized inocula at 45 °C. From the light-optical microscopy observations, the corrosion products formed on the surface of the four samples exhibit distinct morphological features.

Both the biotic and boiled copper coupons exhibit a thick green patina of corrosion products, which appear morphologically similar and develop uniformly across the surface (the brown areas observed on the boiled coupon are attributed to patina detachment during post-exposure handling). At higher magnification, the patina reveals a heterogeneous, multilayered structure consisting of globular aggregates formed atop a thinner underlying layer composed of fine precipitates, suggesting a two-stage growth mechanism (Fig. 6a and b). EDS analyses (Fig. 7a and

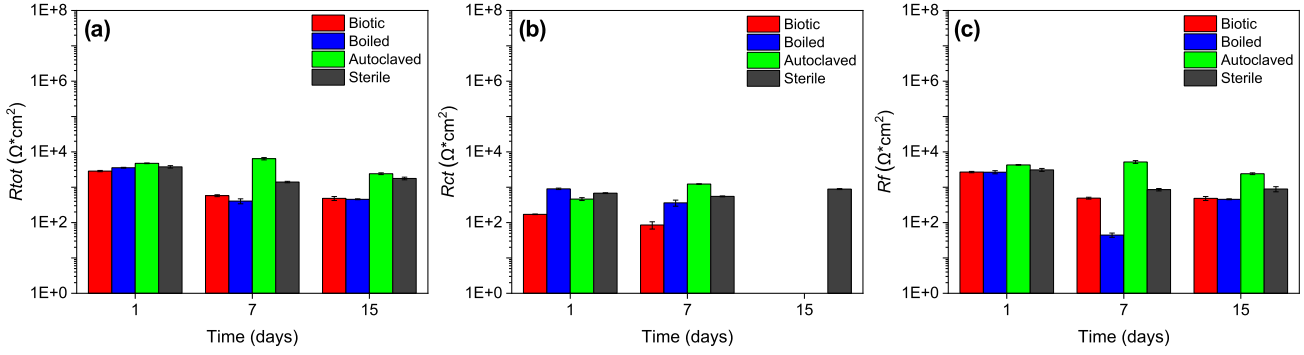

Fig. 4. Evolution of the logarithmic resistance contributions for each condition and exposure time: (a) *Rtot=Rct + Rf*; (b) *Rct*; (c) *Rf*.

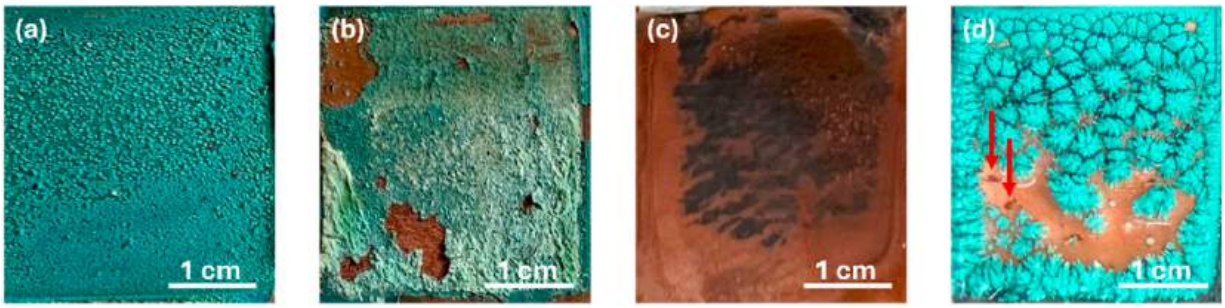

Fig. 5. Optical microscopy images of Cu coupons after 15-days test under microaerophilic conditions in the (a) biotic, (b) boiled, (c) autoclaved and (d) sterile solutions at 45 °C. Arrows on the sterile surface indicate pronounced local corrosion (darker than Cu).

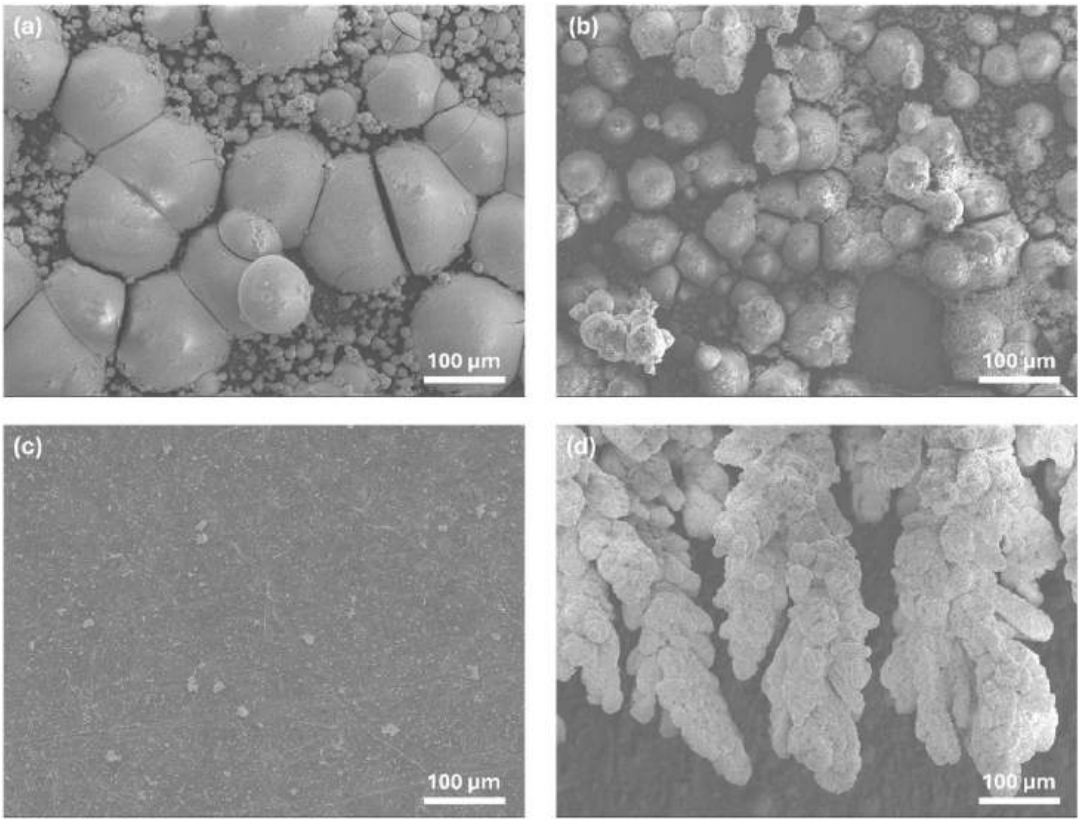

Fig. 6. Scanning electron microscopy images of Cu coupons after 15-day test under microaerophilic conditions in the (a) biotic, (b) boiled, (c) autoclaved and (d) sterile control solutions at 45 °C.

b) indicate the precipitation of distinct corrosion products within these layers.

The globular aggregates are primarily composed of Cu, O, and P, consistent with the formation of copper phosphate phases, such as $Cu_2PO_4(OH)$. In contrast, the underlying layer also contains significant amounts of Cl, suggesting the presence of more complex, chloride-containing phosphate corrosion products. This is even more evident for both conditions from the cross-section images where a thick and uniform phosphate layer is observed on the surface of the coupon (Fig. 8a and b). The sterile sample also shows a greenish to light-blue patina, though its morphology differs noticeably (Fig. 5d). Unlike the biotic and boiled conditions, the outer corrosion film is non-uniform, with clearly visible localized corrosion sites, highlighted by red arrows. The corrosion layer is characterized by distinct acicular (needle-like) structures emerging from a very thin oxidized base layer (Fig. 6d). EDS analyses confirmed the presence of Cl as a major constituent of the corrosion patina, together with Cu and O, suggesting the formation of copper chloride and oxychloride phases (Fig. 7d). Cross-sectional observations further corroborate this stratified corrosion structure, revealing an inner layer primarily composed of copper oxides overlying a more complex, chloride-rich layer of corrosion products (Fig. 8d). In contrast, the coupon immersed in the autoclaved solution displays a markedly less degraded surface. In contrast, the coupon immersed in the autoclaved solution exhibits a markedly less degraded surface. The corrosion layer appears as a thin, uniform brown patina covering the entire surface, with isolated black deposits distributed across the exposed area (Fig. 5c). At higher magnification, the patina is observed to be very thin and compact, predominantly composed of copper oxides, with only rare occurrences of chloride-containing precipitates (Figs. 6c and 7c). This compact and homogeneous surface morphology is indicative of a more passive corrosion behavior and limited corrosion progression. This interpretation is further supported by cross-sectional observations (Fig. 8c), which reveal the presence of a dense, continuous oxide layer at the metal surface that likely acts as a

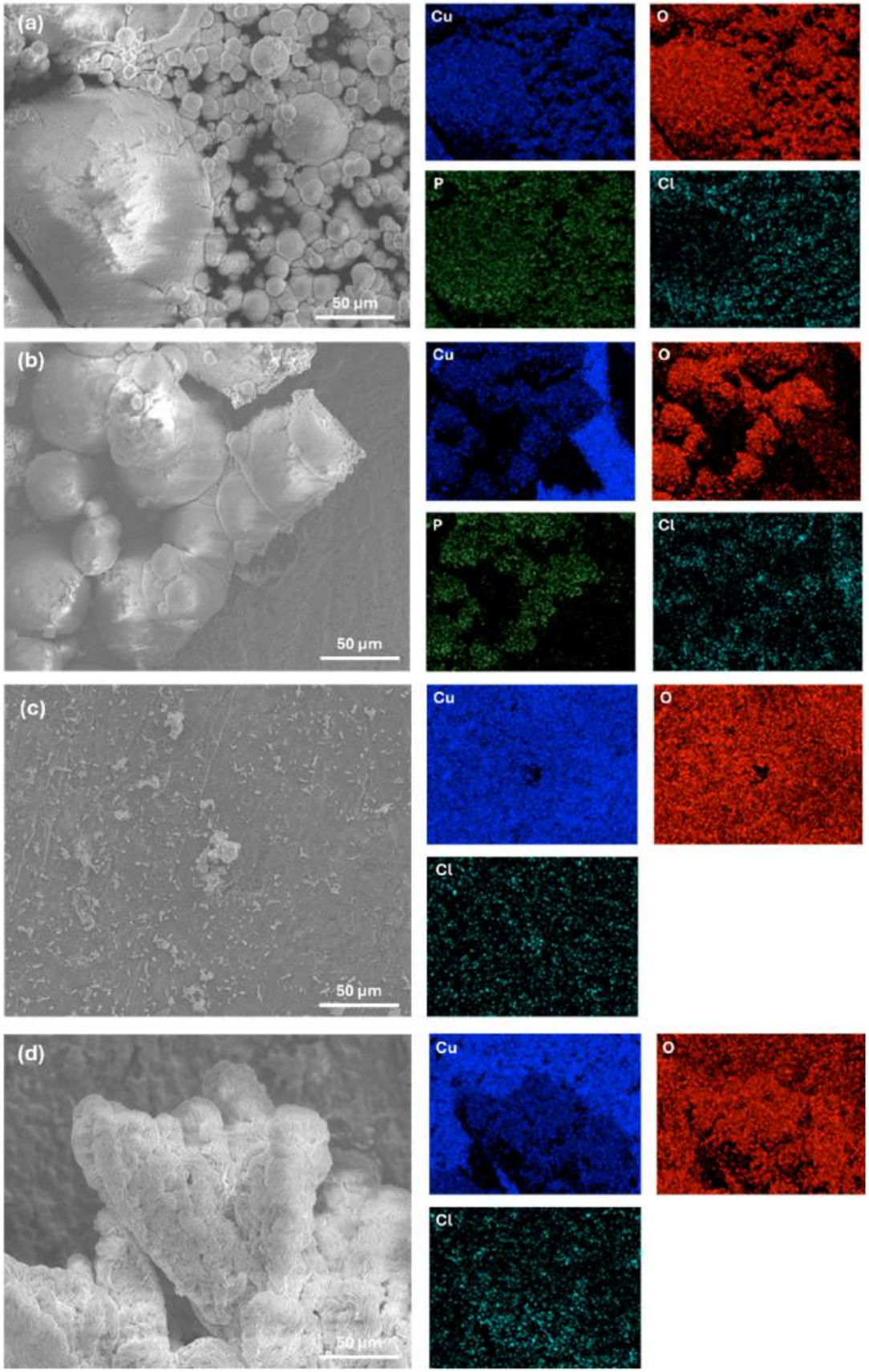

Fig. 7. SEM-EDS images of Cu coupons after 15-day under microaerophilic conditions test in the (a) biotic, (b) boiled, (c) autoclaved and (d) sterile control solutions at 45 °C.

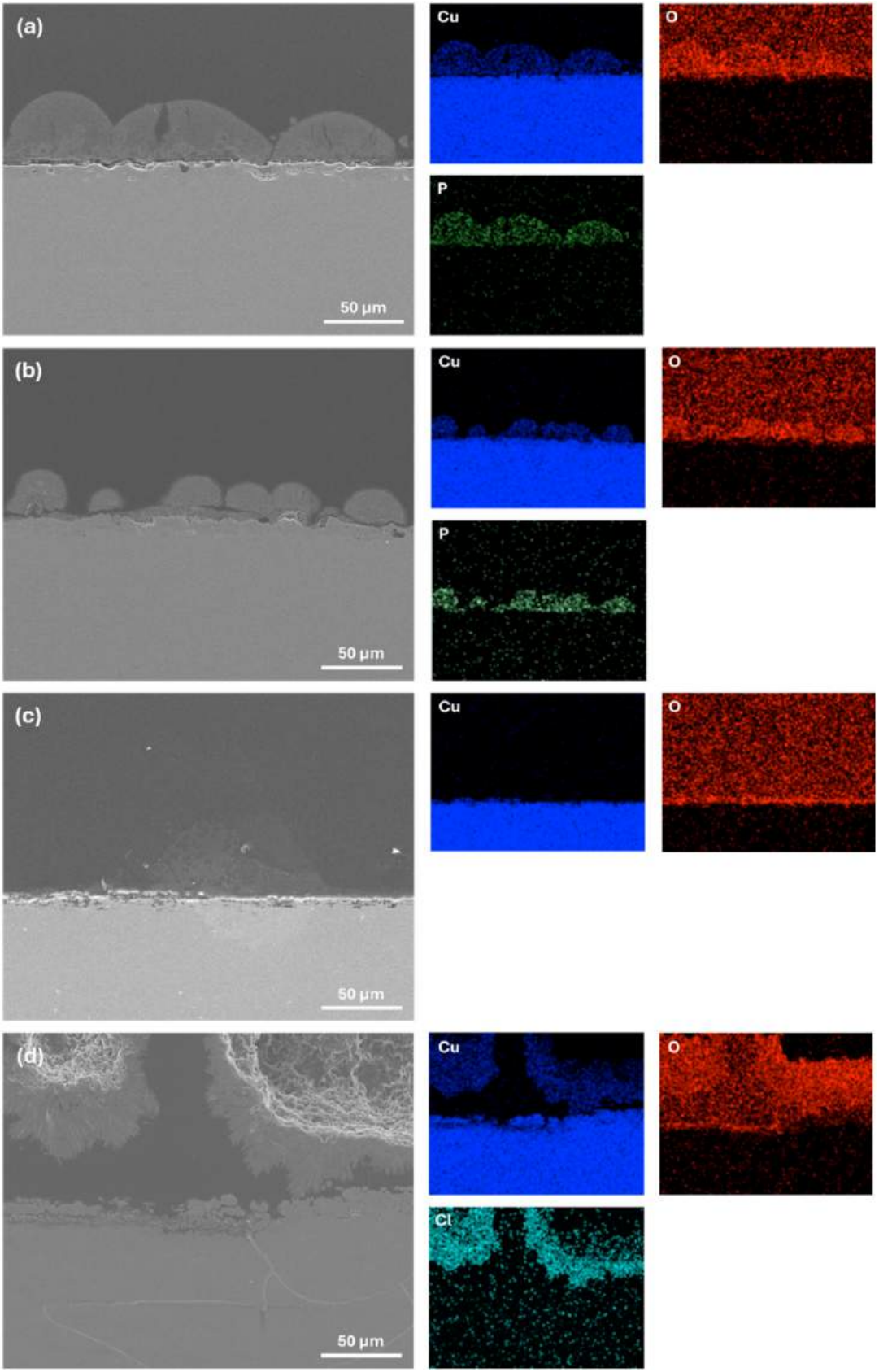

Fig. 8. SEM-EDS images of Cu cross-section after 15-day test under microaerophilic conditions in the (a) biotic, (b) boiled, (c) autoclaved and (d) sterile control solutions at 45 °C.

protective barrier, inhibiting further corrosion.

3.6. Raman spectroscopy

Raman spectroscopy analysis of the copper surfaces after 15 days of immersion (Fig. 9) revealed pronounced differences in the nature of the corrosion products as a function of the immersion conditions, thereby corroborating the trends observed in the EDS analyses. The distinct Raman signatures indicate that the corrosion mechanisms and resulting surface chemistries are strongly influenced by the exposure environment, leading to the formation of different corrosion phases under biotic, boiled, and autoclaved conditions.

In the biotic sample (red curve), intense Raman bands observed at approximately 218, 410, and 520–530 cm^{-1} confirm the formation of cuprite (Cu_2O), while additional peaks in the 350–400 cm^{-1} and 950–1000 cm^{-1} regions are consistent with the formation of $NaCaCu_5(PO_4)_4Cl$ and $Cu_2PO_4(OH)$. These findings indicate a strong interaction between the copper surface, the phosphate-containing medium, and microbial activity, leading to the precipitation of mixed copper-based phosphate compounds. The boiled sample (blue curve) exhibits a spectral fingerprint similar to that of the biotic condition, suggesting that boiling the medium does not fully inhibit microbial activity and continues to promote the formation of comparable corrosion products. In contrast, the autoclaved sample is dominated by spectral features attributable to Cu_2O, with no detectable phosphate-rich phases. Rather than indicating a less severe corrosion process per se, this signature reflects the formation of a chemically distinct and structurally more uniform protective layer. The exclusive presence of Cu_2O, a dense, low-porosity oxide, in the autoclaved condition, combined with its superior electrochemical resistance (*Rp* values consistently highest across both time points), suggests that Cu_2O film integrity, rather than phosphate precipitation, constitutes the primary protective mechanism in this condition. This distinction is mechanistically significant and is discussed further in Section 4.2. The sterile coupon exhibits weak Raman peaks around 430 and 500 cm^{-1}, attributable to Cu–Cl vibrations, characteristic of corrosion in abiotic aqueous environments rather than microbially influenced processes. These features are consistent with the formation of $CuCl_2$ (Crossman, 2006), a common chloride-induced corrosion product of copper (Schmitt et al., 2014). Overall, these results underscore the significant influence of microbial activity and medium composition on the development of complex copper corrosion layers, demonstrating how biotic conditions facilitate the formation of phosphate-rich mixed corrosion products, whereas sterilization limits corrosion predominantly to oxide and chloride species.

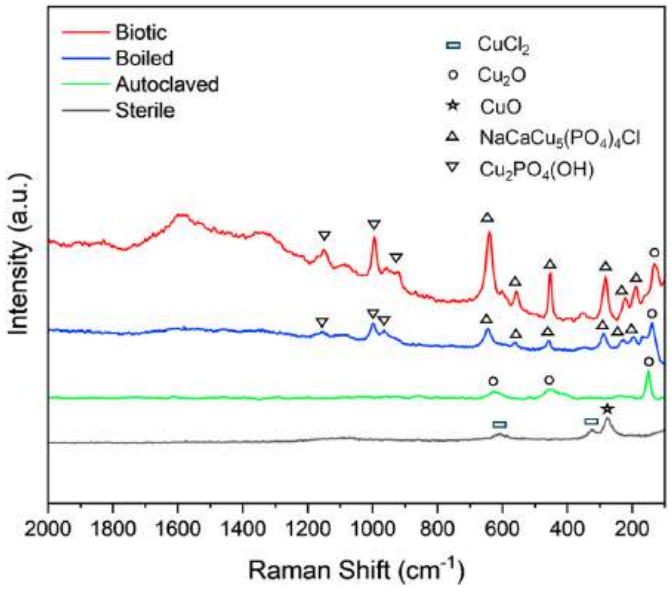

Fig. 9. Raman spectra of Cu coupons after 15-days test under microaerophilic conditions in the biotic, boiled, autoclaved and sterile control solutions at 45 °C.

3.7. Solution chemical analysis

Post-experimental analysis on the solutions allowed the evaluation of potential byproducts of microbial metabolism. The pH measurements revealed values of 6.90 for the biotic test, 6.79 for the boiled sample, 7.09 for the autoclaved sample, and 6.24 for the sterile control, indicating small but notable deviations from the initial pH of 6.96. The ion chromatography analysis (Table 7) shows notable variations in the concentrations of organic acids and carbonates across different conditions over the 15-day test period. In the biotic inoculum, acetate accumulated from below the detection limit to 132.2 mg L^{-1} over the 15-day exposure period. This increase is consistent with active microbial fermentative metabolism, as reported for anaerobic communities with similar composition (McDonald et al., 2013). However, since significant acetate accumulation was also observed in the boiled condition (from 178.1 to 899.2 mg L^{-1}) a purely biological interpretation of acetate production in the biotic condition cannot be made unambiguously. It is plausible that a background abiotic contribution, such as thermally induced hydrolysis of organic volatile fatty acids or residual enzymatic activity, also occurs in the biotic system, albeit at lower levels than in the heat-treated conditions. The biotic acetate signal should therefore be interpreted as consistent with, but not exclusively attributable to, active microbial metabolism.

Conversely, formate was initially present (9.010 mg L^{-1}) but fell below the detection limit (BDL) of the instrument at the end of the test, suggesting its almost complete consumption or conversion by microorganisms, in line with observations of formate utilization as an electron donor in microbial metabolism (Revie and Uhlig, 2008).

In contrast, boiled and autoclaved inocula showed significant increases in acetate concentration, particularly in the boiled condition (from 178.1 to 899.2 mg L^{-1}), which could be attributed to abiotic chemical reactions or residual enzyme activity surviving the thermal treatments (Knight et al., 2010). Formate was mostly absent or present at very low levels, supporting the hypothesis of diminished microbial activity in these conditions. The sterile condition showed no detectable organic acids (except for oxalates), confirming the absence of microbial metabolism.

Oxalate concentrations increased moderately across all samples, with the highest final values detected in boiled and autoclaved inocula, suggesting possible chemical transformations independent of microbial activity, as reported in abiotic aqueous corrosion systems. Carbonates remained relatively stable or increased slightly in the autoclaved samples, while decreasing in the boiled inoculum, which might reflect variations in inorganic carbon equilibria influenced by pH and microbial presence (Jones and Amy, 2002).

The ICP-AES data (Table 8) indicate a significant increase in dissolved copper concentrations in all inocula after 15 days, from trace initial values (e.g., 0.008 mg L^{-1} in biotic) to concentrations exceeding 3 mg L^{-1} in biotic, boiled, and autoclaved samples. This increase suggests active copper corrosion and solubilization during the test period, consistent with the known susceptibility of copper to aqueous corrosion (Chao and Lei, 1995; Muyzer and Stams, 2008). Interestingly, the sterile control showed no initial copper but a final concentration of 7.1 mg L^{-1}, indicating that copper release occurred to a greater extent abiotically, potentially enhanced by chemical corrosion processes in the absence of microbial influence (Drouin et al., 2023).

In the biotic and boiled inocula, the decrease in phosphorous concentration could be attributed to the precipitation of phosphate-based corrosion products, whereas in the autoclaved condition an increase was observed, likely due to the absence of such precipitation or different chemical equilibria. Sulfur levels decreased in biotic and boiled inocula,

Table 8
Inductively coupled plasma – atomic emission spectroscopy analysis of Cu, P and S in biotic, boiled, autoclaved and sterilized (control) inocula. Results of the concentration (ppm) are compared before the start of the test (initial concentration) and after the 15-day of the test (final concentration).

	Biotic		Boiled		Autoclaved		Sterile	
	Concentration (mg L^{-1})[a]							
	Initial	Final	Initial	Final	Initial	Final	Initial	Final
Copper	0.008	3.116	0.013	3.731	0.010	3.090	BDL	7.10
Phosphorous	308.4	208.1	417.1	277.4	420.4	492.9	125.0	100.0
Sulfur	8.174	2.699	3.355	2.182	3.435	4.430	4.20	5.00

[a] *Concentrations below the limit of detection are indicated as "BDL" in the table.*

possibly reflecting microbial sulfate reduction or incorporation into biomass, whereas autoclaved and control samples showed stable or slightly increased sulfur concentrations, consistent with limited biological activity (Chen et al., 2016).

Overall, the solution chemistry data reveal that copper release is governed by a combination of biotic and abiotic processes, whose relative contributions shift depending on the experimental condition. Critically, the sterile control exhibited by far the highest dissolved copper concentration (7.1 mg L^{-1}) despite the complete absence of microbial activity, demonstrating unambiguously that chloride-driven abiotic corrosion represents the most aggressive dissolution pathway in this system. In contrast, all biotic conditions, including the untreated biotic (3.1 mg L^{-1}), boiled (3.7 mg L^{-1}), and autoclaved (3.1 mg L^{-1}), showed substantially lower copper release, consistently pointing to a net moderating influence of the microbial community on cumulative copper dissolution. Phosphorus depletion in the biotic and boiled conditions further corroborates this interpretation, as it reflects the immobilization of dissolved copper into low-solubility phosphate mineral phases, effectively removing it from the corrosive cycle. These findings collectively indicate that the microbial community, regardless of its specific composition, exerts a measurable buffering effect on copper corrosion severity compared to the uninhibited abiotic attack observed under sterile conditions.

Additionally, the formate depletion observed in the biotic inoculum is consistent with its utilization as an electron donor in microbial metabolism, providing a more specific indicator of biological activity than acetate alone. Acetate accumulation, while observed across multiple conditions including the thermally treated ones, likely reflects a combination of microbial and abiotic organic acid generation, the relative contributions of which cannot be fully decoupled from the present dataset. Critically, the highest copper release was recorded in the sterile control (7.1 mg L^{-1}), underscoring that abiotic chloride-driven corrosion, in the complete absence of any microbial or biofilm-mediated process, represents the most aggressive corrosion pathway observed in this study. This finding cautions against overattributing corrosion severity to microbial organic acid production.

3.8. Microbial community composition

Microbial community profiling was performed by 16S rRNA gene NGS (Illumina) on both biofilms and inocula from the four experimental conditions (i.e., biotic, boiled, autoclaved, sterile control). After 15 days, samples from the inoculum, electrode biofilm, and surrounding solution were analyzed. Sterile controls was verified by the absence of growth on LD agar. In contrast, microbial presence was detected in the biotic, boiled, and autoclaved systems.

Fig. 10 shows the relative abundance at the genus level of the bacterial communities in the inoculum prior to the electrochemical tests (*Inocula*), and at the end of the exposure period in the biofilm formed on the metal coupon surface (*Biofilm*), and in the bulk inoculum (*Solution*) for each tested condition (i.e., biotic, boiled and autoclaved). Notably, in all three conditions, a substantial portion of the bacterial communities, ranging from 30% to 60%, is made of genera with a relative abundance lower than 5%. The starting inocula show considerable variation. In the biotic sample, *Alcaligenes* and *Lentilactobacillus* are the most abundant genera, reflecting active roles in nitrogen cycling and fermentation (Zhang et al., 2020; Manaia et al., 2003). Boiling treatment shifts the bacterial community toward heat-tolerant genera like *Tepidiphilus* (19%), a nitrate reducing bacterium belonging to the family Hydrogenophylaceae (Poddar et al., 2014). Members of this genus have been reported in the produced water from thermophilic aerobic digesters (Özdemir et al., 2013), and hot springs (Zhang et al., 2024). In the autoclaved sample there is an increased representation of unclassified bacteria (30%) and the spore-formers *Effusibacillus* (8%), indicating the survival of only the most resilient microorganisms. The biofilm community is significantly enriched with taxa that can tolerate or metabolize

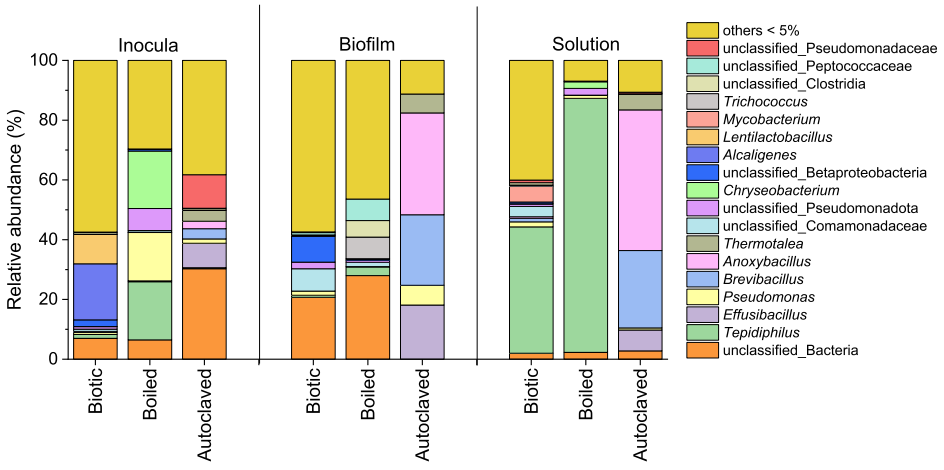

Fig. 10. Bar plot showing the genera relative abundances of bacteria communities of the inoculum not treated (biotic), boiled for 2 h, and autoclaved twice at 121 °C for 20 min.

heavy metals (Scott, 1990). For example, the genera *Anoxybacillus* and *Brevibacillus* are particularly dominant in the autoclaved biofilm, with relative abundances of 34% and 23%, respectively, compared to their low relative abundance in solution. These genera, often known for their spore-forming and thermophilic characteristics, may play a role in forming resilient communities in the presence of copper. Similarly, *Effusibacillus* is found exclusively in the autoclaved biofilm (18%). Additionally, the presence of *Pseudomonas* in biofilm communities from both autoclaved and boiled conditions is noteworthy. *Pseudomonas* species are among the most extensively studied organisms in MIC research owing to their capacity to form electrochemically active biofilms that can accelerate passive film degradation through direct electron transfer mechanisms and the production of redox-active metabolites (Arroussi et al., 2026a). Their detection in the thermally treated inocula suggests that even partial community disruption preserves electrochemically relevant taxa.

In contrast, the solution community is characterized by a high abundance of the genera *Tepidiphilus* and *Anoxybacillus* in the biotic/boiled and autoclaved conditions, respectively. *Tepidiphilus* is predominantly present in the solution of biotic and boiled samples, its relative abundance shifts from 42% in the former and 85% in the latter. Its presence is less relevant in the biofilm, suggesting a preference for a free-floating lifestyle rather than attachments to the Cu electrode. *Anoxybacillus* comprised a remarkable 47% of the autoclaved solution community, indicating its high resilience and ability to survive under high temperature conditions. The observed difference in bacterial community composition and enrichment across treatments highlights a dynamic bacterial response to stressors, with thermal treatments selectively enriching for resilient taxa.

To assess the number of ASVs in each sample, therefore the species richness, the dataset was rarefied at 5685 sequences for the inocula samples, resulting in 431 ASVs in the biotic, 244 in the boiled and 210 in the autoclaved conditions. For the biofilm samples, the dataset was rarefied at 364 sequences, and the number of ASVs resulted 188 in the biotic, 149 in the boiled and 15 in the autoclaved. For the solution samples, the dataset was rarefied at 8564 sequences, and the number of ASVs was 328 in the biotic, 202 in the boiled and 72 in the autoclaved. Cluster analysis based on the Hellinger distance, using ASVs data, shows that the autoclaved samples cluster away from the biotic and boiled samples (Fig. 11). This result indicates that the autoclaving treatment leads to substantially different bacterial communities with respect to the other two conditions.

Fig. 12 shows the genera relative abundance of archaeal communities before and after the tests in each tested condition. In all cases, before and after the exposure period (i.e., inocula and solution), samples are dominated by *Methanotermobacter*, a group of thermophilic hydrogenotrophic methanogens (Feng et al., 1997). In contrast, significant shifts are observed in the biofilm communities formed on the Cu coupon. Both the biotic and the boiled samples share a similar composition, consisting of *Methanospirillum* (35-40%), *Methanosarcina* (17-24%), and members of the order Methanomicrobiales (22%), indicating a stable colonization regardless of the samples. Interestingly, the biofilm from the autoclaved sample exhibits a different archaeal community composition, dominated by *Methanobacterium* (76%). In the solution, the archaeal community of all three samples is dominated by *Methanothermobacter*, reflecting the composition of the initial inoculum.

For the archaeal community, to determine the number of ASVs in each sample, the dataset was rarefied at 110885 sequences for the inocula samples, resulting in 4 ASVs in the biotic, 4 in the boiled, and 3 in the autoclaved conditions. For the biofilm samples, the dataset was rarefied at 1498 sequences, and the number of ASVs was 67 in the biotic, 68 in the boiled, and 17 in the autoclaved. For the solution samples, the dataset was rarefied at 67043 sequences, and the number of ASVs was 4 in the biotic, 5 in the boiled, and 4 in the autoclaved. Cluster analysis shows that the biofilm samples cluster together (Fig. 13), suggesting these samples are more similar with respect to the others. Additionally, the autoclaved inoculum and the autoclaved solution form a distinct cluster. Interestingly, as also reflected from the relative abundance graph, both the biotic and boiled inocula and solutions cluster together, suggesting a similar community composition despite the boiling treatment.

4. Discussion

Data obtained through a multi-faceted approach, including electrochemical monitoring, surface analyses, solution chemistry, and microbial community profiling, clearly indicate that bacterial and archaeal activity exerts a strong, yet distinct, influence on copper corrosion under the different test conditions. Based on the results, it can be inferred that the abundant bacterial populations present in the biotic and boiled systems likely contribute to the initial acceleration of corrosion and delay the onset of mineral stabilization, partially counteracting the archaeal-mediated MIC inhibition mechanisms observed under the autoclaved condition. In particular, the archaeal community detected under autoclaved conditions, dominated by *Methanobacterium sp.* (76%), may mitigate corrosion through several complementary mechanisms. Hydrogenotrophic methanogens can consume H_2 generated at cathodic sites, thereby reducing cathodic depolarization and slowing overall corrosion kinetics. In addition, the archaeal biofilm observed by SEM analysis may act as a physical diffusion barrier limiting chloride transport toward the copper surface and favoring the stability of the compact Cu_2O layer observed in the autoclaved system. Methanogenic metabolism may also locally modify the redox environment and interfacial pH through H_2 and CO_2 consumption, thermodynamically promoting Cu_2O passivation over chloride-induced dissolution. Furthermore, hydrogenotrophic methanogenesis mainly produces CH_4, a non-

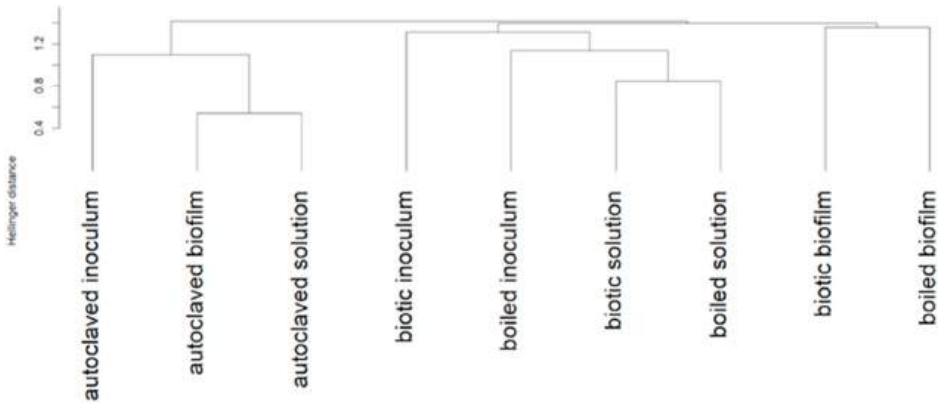

Fig. 11. Hierarchical cluster analysis of bacterial communities based on Hellinger distances.

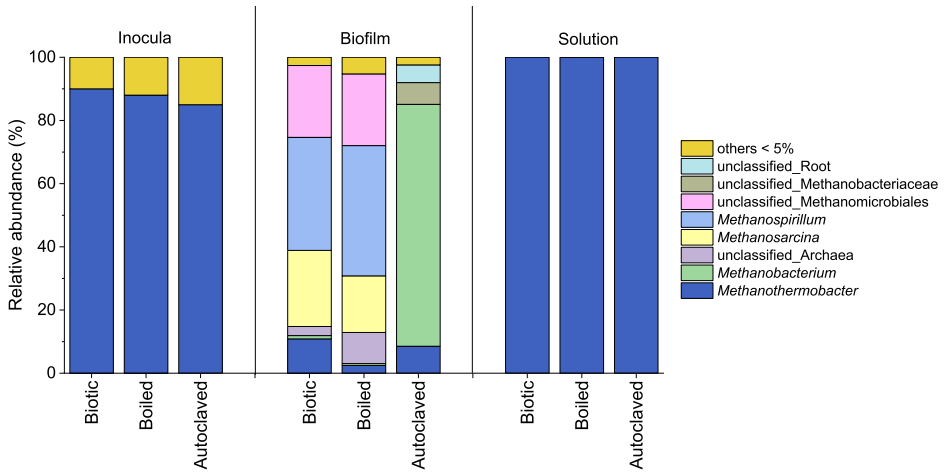

Fig. 12. Bar plot showing the genera relative abundances of archaeal communities of the inoculum before starting the test (left) and of the biofilm (middle) and of the solution (right) after 15 days for the tested conditions.

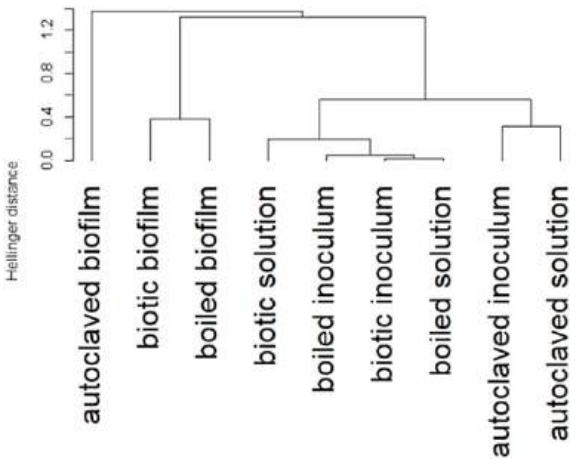

Fig. 13. Hierarchical cluster analysis of archaeal communities on Hellinger distances.

corrosive metabolite that is chemically inert toward copper surfaces, unlike aggressive metabolites such as H_2S produced by sulfate-reducing bacteria. Finally, the selective enrichment of archaeal populations after autoclaving likely suppressed bacterial fermentative and acid-producing pathways that would otherwise promote copper dissolution, resulting in a microbial community shift toward less aggressive electrochemical conditions. Similar MICI mechanisms involving hydrogen consumption, biofilm-mediated protection, redox modification, and microbial community restructuring have been discussed in recent studies on microbial corrosion in pipeline systems (Arroussi et al., 2026b).

Overall results reveal a dynamic interplay between microbiologically influenced corrosion and inhibition. Active microbes and their metabolites transiently modulate copper dissolution in the early phase via anodic reactions coupled to cathodic anaerobic processes, such as proton or cupric ion reduction. Over time, biologically mediated stabilization mechanisms develop either through phosphate mineral precipitation in bacterial-dominated systems or through Cu_2O barrier stabilization, under archaeal-dominated redox control, progressively reducing corrosion severity. In contrast, abiotic systems lack any such self-regulating mechanism: uninhibited chloride attack produces the least protective surface films, the highest copper release, and the most pronounced localized corrosion observed in this study.

4.1. Chloride-driven localized corrosion versus biofilm-assisted mineralization

The distinct trends observed for each coupon over the 15-day exposure provide valuable insight into the different corrosion mechanisms associated with the test conditions. Under biotic conditions, the free corrosion potential initially started at negative values (≈- 0.10 V vs Ag/AgCl sat.) and gradually shifted toward more noble values after 7-8 days. This behavior reflects an early phase dominated by active anodic dissolution of copper, driven by microbially mediated interfacial processes and metabolic acidic by-products, followed by the progressive formation of a protective layer of complex phosphates/chloride compounds that stabilizes for some extent the electrochemical response (Eqs. (2)–(5)). The boiled condition exhibited a similar delayed ennoblement as the biotic condition, suggesting that thermal treatment did not suppress corrosion-relevant microbial activity but instead selected for thermotolerant populations capable of sustaining comparable interfacial processes. In contrast, autoclaved and sterile systems displayed early ennoblement, consistent with the rapid formation of oxides on the Cu surface. The sterile condition, differently than the other conditions, was subsequently affected by potential drops, indicative of an early film destabilization and a transition toward localized corrosion that was more significant than in the other cases.

EIS further clarifies these trends. Biotic and boiled samples displayed initially low impedance responses that evolved toward diffusion- and film-controlled behavior, consistent with the development of thick, porous corrosion layers. Autoclaved samples exhibited comparatively higher and more stable impedance values, reflecting the formation of more compact oxide-dominated patinas. The sterile condition, while initially like autoclaved, evolved toward a heterogeneous electrochemical response with multiple time constants, consistent with the formation and breakdown of stratified corrosion products and localized attacks.

The patina of biotic and boiled samples both consisted of mixed copper-calcium-sodium phosphates, including $NaCaCu_5(PO_4)_4Cl$ and $Cu_2PO_4(OH)$. The formation of these phases can be explained by the progression of the anodic reaction (Eq. (2)):

$$Cu \rightleftarrows Cu^{+} + e^{-} \quad (2)$$

that, in the absence of insoluble and uniform Cu^{+} precipitates, is followed by Eq. (3):

$$2Cu^{+}(aq) \rightleftarrows Cu^{2+} + Cu \quad (3)$$

which, finally, leads to the precipitation of phosphate compounds (Eqs.

4 and 5):

$$2\,Cu^{2+} + PO_4^{3-} + OH^- \rightarrow Cu_2PO_4(OH)\downarrow \quad (4)$$

$$5\,Cu^{2+} + Ca^{2+} + Na^+ + 4PO_4^{3-} + Cl^- \rightarrow NaCaCu_5(PO_4)_4Cl^-\downarrow \quad (5)$$

Phosphorus depletion in the biotic and boiled conditions (up to 100–140 mg L^{-1}) confirmed the formation of phosphate-based corrosion products.

Microbial community analysis revealed that biotic and boiled samples did not show major differences in the composition of the microbial community on both the biofilm and solution after testing. Therefore, it can be inferred that the presence of a rich and comparable bacterial population, including a relevant presence of *Tepidiphilus* genus, likely drove similar metabolic activities, favoring the formation of analogous corrosion products. In these conditions, microbial metabolism played a dual role: an initial metabolic activity (acetogenesis and formate oxidation) accelerated copper dissolution, while the subsequent phosphate precipitation contributed to decreasing corrosion. Acetate accumulation (132.2 mg L^{-1}) and formate consumption in the biotic system point to active syntrophic and methanogenic pathways (Eq. (6)):

$$CH_3COO^- + H^+ \rightleftarrows CH_4 + CO_2 \quad (6)$$

Different than for biotic and boiled coupons, it can be inferred that for the autoclaved condition, the Cu surface was dominated by Cu_2O formation through purely chemical pathways (Eqs. (2), (3), (7)–(9)):

$$2Cu^+ + H_2O \rightleftarrows Cu_2O + 2H^+ \quad (7)$$

$$Cu + 2\,OH^- \rightleftarrows Cu(OH)_2 + 2e^- \quad (8)$$

$$2\,Cu(OH)_2 \rightleftarrows Cu_2O + H_2O + 1/2O_2 \quad (9)$$

Notably, the Cu_2O layer detected by Raman spectroscopy in the autoclaved condition forms a dense, continuous barrier that restricts ionic diffusion to the underlying metal and prevents secondary oxidation to CuO, a phase that is more susceptible to chloride-driven dissolution. The stabilization of Cu_2O rather than CuO in this condition is directly linked to the strictly anaerobic microenvironment maintained by the *Methanobacterium*-dominated archaeal biofilm, which suppresses oxidative reactions at the metal surface. This represents a biologically mediated protective mechanism that is mechanistically distinct from phosphate precipitation: rather than physically blocking ionic transport through a mineral precipitate, it preserves the thermodynamic stability of the most protective oxide phase available on copper under these conditions. It is therefore the Cu_2O film (not phosphate mineralization) that constitutes the primary protective mechanism in the autoclaved condition, and the archaeal community contributes to this protection by sustaining the anaerobic redox environment necessary for its stability. Indeed, the sterile coupon showed a peculiar layer of green/blue deposits of hydrated CuO.

Surface inspection of the sterile samples revealed clear pitting (Fig. 8d), suggesting that the passive oxide layer is unstable in the chloride-rich inoculum. The abundance of Cl^- ions likely promote localized film breakdown and its final transformation in $CuCl_2$ (Eq. (10)). This undermines the protective character of the CuO layer, enhancing pit propagation (Lizoul et al., 2024).

$$Cu^{2+} + 2Cl^- \rightarrow CuCl_2 \quad (10)$$

$$Cu^{2+} + H_2O \rightarrow CuO + 2H^+ \quad (11)$$

These conditions are met when surface acidification occurs, which is consistent with the reaction leading to the formation of CuO (Eq. (11)). The ICP-AES data revealed the highest release occurred in the sterile control (7.1 mg L^{-1}), underscoring the limited protective capacity of purely chemical $Cu(OH)_2$/CuO films.

4.2. Bacterial-driven corrosion enhancement versus archaeal-mediated surface stabilization

Microbial community analysis reveals a strong correlation between community composition and the temporal evolution of copper corrosion behavior, which can be articulated across three distinct phases directly traceable in the electrochemical time-series data.

During the early phase (Day 1), the biotic condition exhibits the lowest *Rp* among all conditions (0.28 ± 0.07 kΩ cm^2), and EIS fitting requires EEC I, a circuit incorporating a Warburg diffusion element, indicating that ion transport limitations are operative from the outset. The OCP in biotic and boiled conditions starts at approximately −0.10 V vs Ag/AgCl, substantially more negative than in the autoclaved condition, reflecting ongoing anodic dissolution driven by metabolically active bacterial populations. Formate depletion and nascent acetate accumulation in the biotic system are consistent with active syntrophic and fermentative metabolism at this stage, which locally modifies the interfacial chemistry, maintains dissolved Cu^{2+} in solution, and suppresses the supersaturation conditions required for oxide precipitation. As discussed in Section 3.7, acetate production likely reflects a combination of microbial and abiotic contributions, and formate depletion is considered the more specific metabolic marker here. This bacterial-dominated early phase is therefore characterized by interfacial chemical perturbation that kinetically delays passivation, as reflected in the low *Rct* value (0.17 ± 0.003 kΩ cm^2) extracted from EEC I fitting at Day 1.

During the intermediate phase (Day 7), the corrosion mechanism in the biotic condition transitions to EEC II (i.e. a two-time-constant circuit) whose second time constant (*Rf* = 0.49 ± 0.03 kΩ cm^2, *CPEf-n* ≈ 0.98) signals the formation of a developing surface film, identified by Raman spectroscopy as mixed copper phosphates. Simultaneously, the OCP in biotic and boiled conditions begins its gradual ennoblement toward more positive values, consistent with partial surface coverage by mineral precipitates. The *Ceff* at Day 7 (130 ± 19 μF cm^{-2}) is markedly lower than at Day 1 (740 ± 28 μF cm^{-2}), reflecting a reduction in electrochemically active surface area as biofilm and mineral phases progressively cover the interface. This intermediate phase marks the onset of the archaeal contribution: as bacterial metabolic intermediates, particularly formate and hydrogen, are consumed by methanogenic archaea enriched in the biofilm, the local redox environment shifts toward conditions more favorable for Cu^{2+} immobilization and mineral precipitation.

During the late phase (Day 15), the biotic condition transitions to EEC III, in which charge transfer and double-layer contributions are no longer resolvable, and the entire impedance response is governed by a *Rf* (0.39 ± 0.09 kΩ cm^2) in series with a *W* element (0.48 ± 0.06 kΩ cm^2). This circuit topology is diagnostic of a surface fully covered by a porous mineral patina through which ion transport is rate-limiting, consistent with the Warburg response visible at low frequencies in the Nyquist plot at Day 15. In the autoclaved condition, the same EEC III topology is reached at Day 15 but with markedly higher *Rf* (0.90 ± 0.01 kΩ cm^2) and *W* (1.5 ± 0.12 kΩ cm^2) values, consistent with the denser, more resistive Cu_2O barrier identified by Raman spectroscopy. The *Rct* in the autoclaved condition increases monotonically from 0.46 kΩ cm^2 at Day 1 to 1.2 kΩ cm^2 at Day 7 before transitioning to full film-controlled behavior at Day 15, a trajectory that contrasts sharply with the declining *Rct* in the biotic condition, and directly reflects the progressive consolidation of the Cu_2O layer under the anaerobic conditions maintained by the archaeal biofilm.

To more explicitly connect the observed community composition to the electrochemical outcomes, a speculative metabolic pathway model is proposed, integrating the 16S rRNA sequencing data with the solution chemistry and surface analysis results.

In the biotic and boiled conditions, the bacterial community is dominated by *Tepidiphilus spp*., thermophilic, nitrate-reducing members of the Hydrogenophilaceae, alongside fermentative taxa including

Alcaligenes and *Lentilactobacillus* in the biotic condition. We propose that *Lentilactobacillus* and related fermenters drive the early-stage acetogenesis observed in solution (acetate accumulation: 132.2 mg L^{-1}), producing organic acids that locally acidify the biofilm-metal interface and shift Cu^{2+} speciation away from supersaturation, thereby suppressing oxide nucleation and sustaining anodic dissolution. Concurrently, *Tepidiphilus*, enriched particularly in the boiled solution at 85% relative abundance, is proposed to act as the primary nitrate-reducing population, coupling the oxidation of formate (which disappears from solution in both biotic and boiled conditions) to nitrate reduction. This reaction consumes a key electron donor at the interface, generating local alkalinity gradients that, together with the phosphate-rich medium, progressively create conditions favorable for copper phosphate precipitation (Eqs. 4 and 5). The decline in *Rct* observed in EIS between Day 1 and Day 7 under biotic conditions (from 0.17 to 0.086 kΩ cm^2) is consistent with the production of redox-active metabolic intermediates that facilitate interfacial electron transfer, possibly including flavin-type mediators or reduced quinone species associated with Gram-negative respiratory chains.

In the biofilm of biotic and boiled conditions, the archaeal community is dominated by *Methanospirillum* (35–40%), *Methanosarcina* (17–24%), and *Methanomicrobiales* (~22%). *Methanospirillum* is a hydrogenotrophic methanogen that consumes H_2 and CO_2 to produce CH_4, while *Methanosarcina* is metabolically versatile, capable of both hydrogenotrophic and acetoclastic methanogenesis. We propose that these archaea act as terminal electron sinks in the syntrophic network established at the biofilm-metal interface: by consuming H_2 produced by bacterial fermentation and formate oxidation, they maintain thermodynamically favorable conditions for bacterial metabolism, sustaining the syntrophic partnership (Eq. (6)). Critically, this H_2 consumption by methanogens prevents the accumulation of dissolved H_2 at the copper surface, thereby suppressing the direct cathodic depolarization mechanism (H_2-mediated electron uptake) that has been identified as a key MIC pathway in other systems (Li et al., 2018). As the biofilm matures and the archaeal community becomes more established, the progressive removal of H_2 and formate shifts the local equilibrium toward Cu^{2+} immobilization and phosphate mineral precipitation, consistent with the transition to EEC III at Day 15.

In the autoclaved condition, the archaeal biofilm is instead dominated by *Methanobacterium* (76%), a strict hydrogenotrophic methanogen with a narrower metabolic repertoire. In the near-complete absence of a bacterial community capable of generating fermentative or acidogenic metabolites, the interfacial chemistry is governed primarily by the redox-consuming activity of *Methanobacterium*, which maintains H_2 and O_2 concentrations at the metal surface below the threshold for CuO formation. This strictly anaerobic microenvironment stabilizes Cu_2O as the thermodynamically preferred oxide phase and prevents its conversion to CuO, a phase that, as discussed in Section 4.1, is susceptible to chloride-driven dissolution and pitting. The monotonic increase in *Rct* from Day 1 (0.46 kΩ cm^2) to Day 7 (1.2 kΩ cm^2) in the autoclaved condition, followed by the transition to a compact film-dominated response at Day 15 (Rf = 0.90 kΩ cm^2), is fully consistent with this model: the absence of bacterially produced corrosive metabolites allows the Cu_2O layer to consolidate undisturbed, while the archaeal biofilm passively maintains the redox conditions necessary for its long-term stability.

This integrated metabolic model, while necessarily speculative given the absence of transcriptomic or proteomic data, provides a mechanistically coherent framework that reconciles the community composition data with the electrochemical, surface, and solution chemistry observations across all three phases of the experiment. It also generates testable hypotheses, in particular, that selective inhibition of *Tepidiphilus* nitrate reduction or *Methanobacterium* hydrogenotrophic activity should predictably shift the corrosion outcome toward more aggressive dissolution, which could be addressed in future work combining metatranscriptomics with electrochemical monitoring.

Thus, while bacterial activity modulates corrosion kinetics during the early exposure phase, sustaining copper dissolution and delaying passivation, this effect must be contextualized against the overall corrosion outcome. The sterile condition, devoid of any microbial community, exhibited the highest copper release (7.1 mg L^{-1}) and the most severe localized attack, demonstrating that uninhibited abiotic chloride-driven corrosion is ultimately more damaging than the biologically mediated processes occurring under biotic conditions. Bacterial activity should therefore be understood as an early-stage modulator rather than a net corrosion accelerator; its contribution is progressively counteracted and ultimately superseded by the archaeal-driven patina stabilization that develops over time. This is further supported by microbial community profiling. Biotic and boiled systems converged toward similar bacterial and archaeal biofilm compositions despite different initial treatments, consistent with their similar corrosion products and electrochemical signatures. In contrast, autoclaving resulted in a simplified microbial community dominated by resilient thermophilic archaea taxa, correlating with a distinct corrosion phenotype characterized by oxide-dominated, more protective films. Notably, the sterile system-lacking both bacterial and archaeal biofilms exhibited the most aggressive copper release and localized corrosion, underscoring that abiotic chloride-driven corrosion can exceed biotic corrosion severity when biologically mediated immobilization pathways are absent.

Overall, these results reveal that copper corrosion in the analyzed systems is dominated by a thermal-dependent transition governed by microbial functional balance, which can drive the corrosion process in terms of microbially influenced corrosion or inhibition. Over longer exposure times, biologically mediated stabilization mechanisms progressively redirected corrosion from a charge-transfer-controlled regime toward a diffusion-limited one (Fig. 14): through phosphate mineral precipitation in mixed bacterial-archaeal communities, and through Cu_2O barrier consolidation under archaeal-dominated redox control. While this mineral layer does not provide passivation in the strict electrochemical sense, it effectively reduces the rate of localized ionic attack and suppresses the pitting-type corrosion characteristic of the sterile condition. The transition from MIC to MICI observed here is therefore not a binary switch, but a time-dependent continuum driven by the progressive restructuring of the microbial community and its metabolic outputs. Critically, this transition results in a net corrosion outcome that is less severe than that observed under purely abiotic conditions, where chloride ions act unopposed on the copper surface. The combined microbial community, bacterial and archaeal components alike, should therefore be recognized as exerting a comparatively protective influence relative to the sterile control, even if this protection is partial and mechanistically distinct from classical passivation. This nuanced interaction is particularly relevant for predicting copper durability in warm, anaerobic, chloride-containing environments.

5. Conclusion

This study yields four principal conclusions of broad relevance to microbial corrosion science and materials engineering in thermophilic environments. First, standard autoclaving protocols (121 °C, 20 min) do not achieve complete sterilization of methanation-derived inocula. Thermal treatments act primarily as community-selective pressures, enriching for thermotolerant and spore-forming taxa, and should not be assumed to produce microbiologically inert conditions in systems originating from thermophilic biotechnological processes. Second, two mechanistically distinct pathways of MICI are operative in this system, depending on community composition. In archaeal-dominated conditions (autoclaved), protection arises from the stabilization of a dense Cu_2O barrier layer maintained by strictly anaerobic redox conditions; in mixed bacterial-archaeal communities (biotic, boiled), partial protection derives from diffusion resistance introduced by porous copper phosphate mineral precipitates. These represent condition-dependent

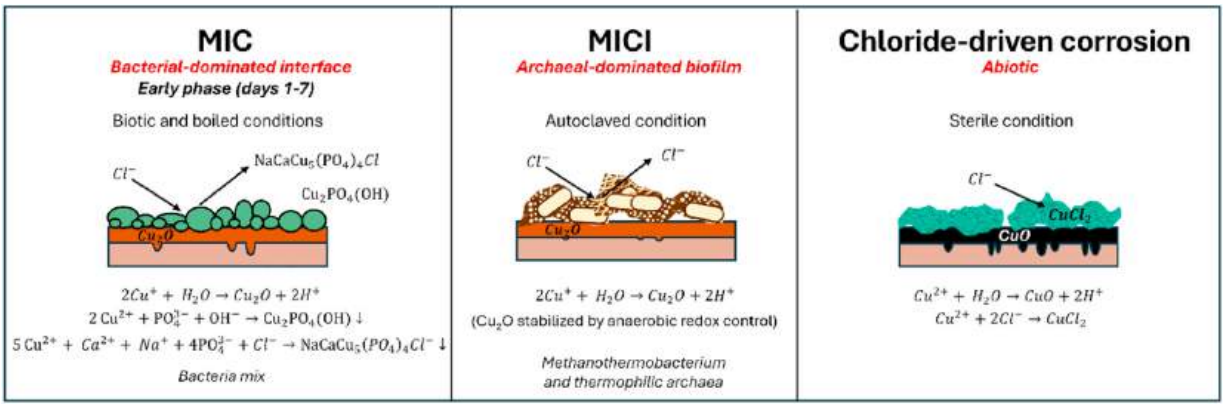

Fig. 14. Mechanistic schematic of thermally enriched bacteria and archaea impact on copper: bacterial activity is primarily associated with early-stage (days 1-7) electrochemical perturbation of the copper interface, whereas archaeal-dominated biofilms promote chemically mediated mineralization leading to MICI-type behavior. In both cases, the net copper release under biotic conditions remains substantially lower than under sterile, chloride-dominated abiotic attack, underscoring the overall moderating role of the microbial community.

MICI mechanisms that should not be conflated. Third, the net corrosion outcome, quantified by dissolved copper release, is consistently lower under all biotic conditions (3.1–3.7 mg L^{-1}) than under the sterile control (7.1 mg L^{-1}), demonstrating that the microbial community as a whole exerts a moderating influence on copper dissolution relative to uninhibited abiotic chloride-driven attack. Early-stage electrochemical perturbation of the interface by bacterial activity does not translate into greater cumulative metal loss. Fourth, the mechanistic framework established here, encompassing thermal community selection, time-resolved MIC-to-MICI transition, and the dual role of bacteria and archaea, is directly transferable to any warm, anoxic, chloride-containing environment, including deep marine hydrothermal settings, engineered biogas systems, and heat recovery infrastructure, where thermophilic consortia interact with copper-based materials. From a practical standpoint, these findings have direct implications for the design and maintenance of copper-based infrastructure operating in warm, anoxic, and chloride-containing environments. In biogas and biological methanation systems, the inherent thermophilic microbial consortia should not be regarded as purely detrimental agents; rather, their community composition can be exploited as a controllable variable to steer corrosion outcomes. Thermal pre-treatment of recirculating fluids, such as a single boiling step, preserves a protective, phosphate-mineralizing community while eliminating the most aggressive mesophilic populations. Conversely, more stringent sterilization should be avoided in systems where microbial MICI is advantageous, as the sterile condition consistently produced the highest copper release. The dual-pathway MICI framework (Cu_2O barrier vs. phosphate diffusion layer) provides a rational basis for selecting operating temperatures and community management strategies to minimize copper dissolution and extend component lifetime in green hydrogen and renewable energy infrastructure.

CRediT authorship contribution statement

Elena Cazzulani: Data curation, Formal analysis, Investigation, Writing – original draft. **Giorgia Ghiara:** Formal analysis, Investigation, Writing – original draft. **Gabriella Caucia:** Data curation, Formal analysis, Investigation. **Andrea Franzetti:** Data curation, Formal analysis, Validation. **Marcella Balordi:** Funding acquisition, Resources. **Paolo Fedeli:** Formal analysis, Investigation. **Francesco Pini:** Data curation, Investigation. **Pierangela Cristiani:** Conceptualization, Data curation, Funding acquisition, Methodology, Supervision, Writing – review & editing. **Gian Luca Chiarello:** Conceptualization, Funding acquisition, Supervision, Writing – review & editing.

Declaration of competing interest

The authors declare that they have no known competing financial interests or personal relationships that could have appeared to influence the work reported in this paper.

Acknowledgments

Research activities were carried out in the context of the National Recovery and Resilience Plan (PNRR) - Mission 2 - Component 2 - Investment 3.5 "Research and Development on Hydrogen", funded by the European Union - next generation EU, and performed in implementation of the Operative Research Program (POR) approved by the ministry of ecological transition on 06.27.2022.

Data availability

Data will be made available on request.

References

Amendola, R., Acharjee, A., 2022. Microbiologically influenced corrosion of copper and its alloys in anaerobic aqueous environments: a review. Front. Microbiol. 13, 806688. https://doi.org/10.3389/fmicb.2022.806688.

Arroussi, M., Al-Athel, K., Ulhaq Toor, I., Zhang, R., 2025a. Interspecies electron transfer of mixed-species biofilms in microbial corrosion of metals: mechanisms and mitigation strategies. World J. Microbiol. Biotechnol. 41, 375. https://doi.org/10.1007/s11274-025-04599-x.

Arroussi, M., Jia, Q., Bai, C., Zhang, S., Zhao, J., Xia, Z., Zhang, Z., Yang, K., Yang, R., 2022. Inhibition effect on microbiologically influenced corrosion of Ti-6Al-4V-5Cu alloy against marine bacterium Pseudomonas aeruginosa. J. Mater. Sci. Technol. 109, 282–296. https://doi.org/10.1016/j.jmst.2021.08.084.

Arroussi, M., Jia, Q., Ter-Ovanessian, B., Yang, K., Bai, C., Wu, J., Wang, P., 2024. Investigation on the Passive Behavior of Ti-9Mn alloy in 3.5 wt% NaCl Solution. J. Electrochem. Soc. 171, 053503. https://doi.org/10.1149/1945-7111/ad4a0a.

Arroussi, M., Ulhaq Toor, I., Ma, W., Shams, A., Al-Athel, K., 2026b. Advances in understanding microbial corrosion of oil pipelines. Discov. Bact. 3, 8. https://doi.org/10.1007/s44351-026-00046-w.

Arroussi, M., Yang, K., Jia, Q., Bai, C., Wang, W., Zhang, R., 2026a. Mechanistic insights into Pseudomonas aeruginosa biofilm-driven passive film degradation of Ti-9Mn alloy in marine environment. Corros. Commun. https://doi.org/10.1016/j.corcom.2026.01.010. S2667266926000629.

Arroussi, M., Yang, K., Shams, A., Toor, I.U.H., Wei, B., 2025b. Advances in microbial corrosion of metals induced via extracellular electron transfer by Shewanella oneidensis MR-1. npj Mater. Degrad. 9, 47. https://doi.org/10.1038/s41529-025-00580-z.

Arroussi, M., Zhao, J., Bai, C., Zhang, S., Xia, Z., Jia, Q., Yang, K., Yang, R., 2023. Evaluation of inhibition effect on microbiologically influenced corrosion of Ti-5Cu alloy against marine Bacillus vietnamensis biofilm. Bioelectrochemistry 149, 108265. https://doi.org/10.1016/j.bioelechem.2022.108265.

Bassani, I., Kougias, P.G., Treu, L., Angelidaki, I., 2015. Biogas upgrading via hydrogenotrophic methanogenesis in two-stage continuous stirred tank reactors at

mesophilic and thermophilic conditions. Environ. Sci. Technol. 49, 12585–12593. https://doi.org/10.1021/acs.est.5b03451.
Bougrier, C., Delgenès, J.P., Carrère, H., 2008. Effects of thermal treatments on five different waste activated sludge samples solubilisation, physical properties and anaerobic digestion. Chem. Eng. J. 139, 236–244. https://doi.org/10.1016/j.cej.2007.07.099.
Brug, G.J., van den Eeden, A.L.G., Sluyters-Rehbach, M., Sluyters, J.H., 1984. The analysis of electrode impedances complicated by the presence of a constant phase element. J. Electroanal. Chem. Interfacial Electrochem. 176, 275–295. https://doi.org/10.1016/S0022-0728(84)80324-1.
Callahan, B.J., McMurdie, P.J., Rosen, M.J., Han, A.W., Johnson, A.J.A., Holmes, S.P., 2016. DADA2: High-resolution sample inference from Illumina amplicon data. Nat. Methods 13, 581–583. https://doi.org/10.1038/nmeth.3869.
Cazzulani, E., Caucia, G., Chiarello, G.L., Franzetti, A., Pittino, F., Atanassov, P., Cristiani, P., 2025. Harnessing hyperthermophilic metabolism to boost bioelectrochemical systems: key thermodynamic challenges. Chem. Eng. J. 522, 167756. https://doi.org/10.1016/j.cej.2025.167756.
Cazzulani, E., Ghiara, G., Pittino, F., Franzetti, A., Balordi, M., Fedeli, P., Malgrati, E., Cristiani, P., Chiarello, G.L., 2026. Selective microbial enrichment by thermal treatments controls brass corrosion in methanation environments. Corros. Sci. 264, 113731. https://doi.org/10.1016/j.corsci.2026.113731.
Chao, T.S., Lei, T.F., 1995. Crossover Phenomenon in Oxidation Rates of the (110) and (111) Orientations of Silicon in N 2 O. J. Electrochem. Soc. 142, L34–L35. https://doi.org/10.1149/1.2048576.
Chen, J., Gu, S., Hao, H., Chen, J., 2016. Characteristics and metabolic pathway of Alcaligenes sp. TB for simultaneous heterotrophic nitrification-aerobic denitrification. Appl. Microbiol. Biotechnol. 100, 9787–9794. https://doi.org/10.1007/s00253-016-7840-x.
Chen, S., Wang, P., Zhang, D., 2014. Corrosion behavior of copper under biofilm of sulfate-reducing bacteria. Corros. Sci. 87, 407–415. https://doi.org/10.1016/j.corsci.2014.07.001.
Cheng, Z., Li, S., Wang, M., Ma, X., 2024. Application of copper-based compounds in energy conversion and catalysis. In: Fernández González, D. (Ed.), Copper Overview - from Historical Aspects to Applications. IntechOpen. https://doi.org/10.5772/intechopen.1004179.
Cristiani, P., Moradi, M., Basseguy, R., Macdonald, D., Gu, T., Zhang, D., Wharton, J., Xu, D., 2025. Fundamentals and critical appraisal of electrochemical techniques for investigating microbial corrosion. Corros. Sci. 246, 112694. https://doi.org/10.1016/j.corsci.2025.112694.
Cristiani, P., Perboni, G., 2014. Antifouling strategies and corrosion control in cooling circuits. Bioelectrochemistry 97, 120–126. https://doi.org/10.1016/j.bioelechem.2014.01.002.
Crossman, L., 2006. Budget genomes. Nat. Rev. Microbiol. 4, 326–327. https://doi.org/10.1038/nrmicro1396.
Díaz, E.E., Stams, A.J.M., Amils, R., Sanz, J.L., 2006. Phenotypic properties and microbial diversity of methanogenic granules from a full-scale upflow Anaerobic Sludge bed reactor treating brewery wastewater. Appl. Environ. Microbiol. 72, 4942–4949. https://doi.org/10.1128/AEM.02985-05.
Drouin, P., Da Silva, É.B., Tremblay, J., Chevaux, E., Apper, E., Castex, M., 2023. Inoculation with Lentilactobacillus buchneri alone or in combination with Lentilactobacillus hilgardii modifies gene expression, fermentation profile, and starch digestibility in high-moisture corn. Front. Microbiol. 14, 1253588. https://doi.org/10.3389/fmicb.2023.1253588.
Edwards, M., Hidmi, L., Gladwell, D., 2002. Phosphate inhibition of soluble copper corrosion by-product release. Corros. Sci. 44, 1057–1071. https://doi.org/10.1016/S0010-938X(01)00112-3.
Feng, Y., Siow, K.-S., Teo, W.-K., Tan, K.-L., Hsieh, A.-K., 1997. Corrosion mechanisms and products of copper in aqueous solutions at various pH values. Corrosion 53, 389–398. https://doi.org/10.5006/1.3280482.
Gagliano, M.C., Braguglia, C.M., Gianico, A., Mininni, G., Nakamura, K., Rossetti, S., 2015. Thermophilic anaerobic digestion of thermal pretreated sludge: role of microbial community structure and correlation with process performances. Water Res. 68, 498–509. https://doi.org/10.1016/j.watres.2014.10.031.
Garcia, F., Leonor Rivera Lopez, A., Campos Guillén, J., Hernández Sandoval, L., Regalado González, C., Castaño, V., 2012. Corrosion Inhibition in Copper by Isolated Bacteria, Anti-corrosion Methods and Materials, vol. 59, pp. 10–17. https://doi.org/10.1108/00035591211190490.
Ghiara, G., Spotorno, R., Delsante, S., Formicola, F., Franzetti, A., Cristiani, P., 2022. Opposite corrosion behaviour of aluminum bronze induced by Pseudomonas fluorescens and its metabolites. Corros. Sci. 208, 110656. https://doi.org/10.1016/j.corsci.2022.110656.
Ghiara, G., Spotorno, R., Delsante, S., Tassistro, G., Piccardo, P., Cristiani, P., 2019. Dezincification inhibition of a food processing brass OT60 in presence of Pseudomonas fluorescens. Corros. Sci. 157, 370–381. https://doi.org/10.1016/j.corsci.2019.06.003.
Ghiara, G., Spotorno, R., Trasatti, S.P., Cristiani, P., 2018. Effect of Pseudomonas fluorescens on the electrochemical behaviour of a single-phase Cu-Sn modern bronze. Corros. Sci. 139, 227–234. https://doi.org/10.1016/j.corsci.2018.05.009.
Glarum, S.H., Marshall, J.H., 1985. The anodic dissolution of copper into phosphoric acid: i . Voltammetric and oscillatory behavior. J. Electrochem. Soc. 132, 2872–2878. https://doi.org/10.1149/1.2113686.
Harrison, J.J., Ceri, H., Turner, R.J., 2007. Multimetal resistance and tolerance in microbial biofilms. Nat. Rev. Microbiol. 5, 928–938. https://doi.org/10.1038/nrmicro1774.
Itzhak, D., Dinstein, I., Zilberberg, T., 1981. Pitting corrosion evaluation by computer image processing. Corros. Sci. 21, 17–22. https://doi.org/10.1016/0010-938X(81)90059-7.
Jankowski, J., Juchniewicz, R., 1980. A four-point method for corrosion rate determination. Corros. Sci. 20, 841–851. https://doi.org/10.1016/0010-938X(80)90118-3.
Jones, D.A., Amy, P.S., 2002. A thermodynamic interpretation of microbiologically influenced corrosion. Corrosion 58, 638–645. https://doi.org/10.5006/1.3287692.
Knight, S.P., Birbilis, N., Muddle, B.C., Trueman, A.R., Lynch, S.P., 2010. Correlations between intergranular stress corrosion cracking, grain-boundary microchemistry, and grain-boundary electrochemistry for al–zn–mg–cu alloys. Corros. Sci. 52, 4073–4080. https://doi.org/10.1016/j.corsci.2010.08.024.
Kouakou, A.R., Kouadio, M.C., Kouakou, V., Konan, G.R., Ehouman, A.D., Diarrassouba, A.S., Niamien, P.M., Yao, B., 2024. Mitigating corrosion in activated carbon purified biogas: a case Study of copper and aluminum metals. Orient. J. Chem. 40, 666–672. https://doi.org/10.13005/ojc/400305.
Lee, Y.-H., Kim, Y.-W., Lim, J.-M., Kang, U.-S., Kim, J.-G., 2025. Effects of environmental factors on copper corrosion in an aerobic deep geological repository. npj Mater. Degrad. 10, 10. https://doi.org/10.1038/s41529-025-00722-3.
Li, Y., Xu, D., Chen, C., Li, X., Jia, R., Zhang, D., Sand, W., Wang, F., Gu, T., 2018. Anaerobic microbiologically influenced corrosion mechanisms interpreted using bioenergetics and bioelectrochemistry: a review. J. Mater. Sci. Technol. 34, 1713–1718. https://doi.org/10.1016/j.jmst.2018.02.023.
Little, B.J., Hinks, J., Blackwood, D.J., 2020. Microbially influenced corrosion: towards an interdisciplinary perspective on mechanisms. Int. Biodeterior. Biodegrad. 154, 105062. https://doi.org/10.1016/j.ibiod.2020.105062.
Little, B.J., Lee, J.S., 2014. Microbiologically influenced corrosion: an update. Int. Mater. Rev. 59, 384–393. https://doi.org/10.1179/1743280414Y.0000000035.
Lizoul, B., Mortadi, A., El Hafidi, E.M., Kounbach, S., Elmelouky, A., Chahid, E.G., 2024. Exploring the interactions of apatitic tricalcium phosphate with copper ions: Time-resolved structural transformations and electrical property insights. Solid State Ionics 410, 116552. https://doi.org/10.1016/j.ssi.2024.116552.
Luo, G., Angelidaki, I., 2012. Integrated biogas upgrading and hydrogen utilization in an anaerobic reactor containing enriched hydrogenotrophic methanogenic culture. Biotechnol. Bioeng. 109, 2729–2736. https://doi.org/10.1002/bit.24557.
Lytle, D.A., Nadagouda, M.N., 2010. A comprehensive investigation of copper pitting corrosion in a drinking water distribution system. Corros. Sci. 52, 1927–1938. https://doi.org/10.1016/j.corsci.2010.02.013.
Manaia, C.M., Nogales, B., Nunes, O.C., 2003. Tepidiphilus margaritifer gen. nov., sp. Nov., isolated from a thermophilic aerobic digester. Int. J. Syst. Evol. Microbiol. 53, 1405–1410. https://doi.org/10.1099/ijs.0.02538-0.
Mansfeld, F., 2007. The interaction of bacteria and metal surfaces. Electrochim. Acta 52, 7670–7680. https://doi.org/10.1016/j.electacta.2007.05.006.
Mansfeld, F., Hsu, C.H., Sun, Z., Örnek, D., Wood, T.K., 2002a. *Technical Note:* Ennoblement— A common phenomenon? Corrosion 58, 187–191. https://doi.org/10.5006/1.3279868.
Mansfeld, F., Hsu, H., Örnek, D., Wood, T.K., Syrett, B.C., 2002b. Corrosion control using regenerative biofilms on aluminum 2024 and brass in different media. J. Electrochem. Soc. 149, B130. https://doi.org/10.1149/1.1456922.
Marquis, R.E., Sim, J., Shin, S.Y., 1994. Molecular mechanisms of resistance to heat and oxidative damage. J. Appl. Bacteriol. 76. https://doi.org/10.1111/j.1365-2672.1994.tb04356.x.
McDonald, J.A.K., Schroeter, K., Fuentes, S., Heikamp-deJong, I., Khursigara, C.M., De Vos, W.M., Allen-Vercoe, E., 2013. Evaluation of microbial community reproducibility, stability and composition in a human distal gut chemostat model. J. Microbiol. Methods 95, 167–174. https://doi.org/10.1016/j.mimet.2013.08.008.
Medeiros, F.E.O., Araújo, B.S., Ayala, A.P., 2018. Raman spectroscopy investigation of the thermal stability of the multiferroic CuCl2 and its hydrated form. Vib. Spectrosc. 99, 1–6. https://doi.org/10.1016/j.vibspec.2018.08.006.
Moradi, M., Ghiara, G., Spotorno, R., Xu, D., Cristiani, P., 2022. Understanding biofilm impact on electrochemical impedance spectroscopy analyses in microbial corrosion and microbial corrosion inhibition phenomena. Electrochim. Acta 426, 140803. https://doi.org/10.1016/j.electacta.2022.140803.
Muyzer, G., Stams, A.J.M., 2008. The ecology and biotechnology of sulphate-reducing bacteria. Nat. Rev. Microbiol. 6, 441–454. https://doi.org/10.1038/nrmicro1892.
Nagiub, A., Mansfeld, F., 2002. Evaluation of microbiologically influenced corrosion inhibition (MICI) with EIS and ENA. Electrochim. Acta 47, 2319–2333. https://doi.org/10.1016/S0013-4686(02)00082-8.
Orazem, M.E., Tribollet, B., 2008. Electrochemical Impedance Spectroscopy. Wiley. https://doi.org/10.1002/9780470381588.
Papirio, S., Villa-Gomez, D.K., Esposito, G., Pirozzi, F., Lens, P.N.L., 2013. Acid mine drainage treatment in fluidized-bed bioreactors by sulfate-reducing bacteria: a critical review. Crit. Rev. Environ. Sci. Technol. 43, 2545–2580. https://doi.org/10.1080/10643389.2012.694328.
Perez, N., 2016. Electrochemistry and Corrosion Science. Springer International Publishing, Cham. https://doi.org/10.1007/978-3-319-24847-9.
Pikuta, E.V., Hoover, R.B., Tang, J., 2007. Microbial extremophiles at the limits of life. Crit. Rev. Microbiol. 33, 183–209. https://doi.org/10.1080/10408410701451948.
Pincam, T., Liu, Y.-Q., Short, M., Guo, B., Sadhukhan, J., Bywater, A., 2026. Challenging conventional temperature ranges in anaerobic digestion: intermediate (45 °C) as general optimum with feedstock-dependent performance differences from mesophilic (35 °C) and thermophilic (55 °C) conditions. Bioresour. Technol. 441, 133609. https://doi.org/10.1016/j.biortech.2025.133609.
Poddar, A., Lepcha, R.T., Das, S.K., 2014. Taxonomic study of the genus Tepidiphilus: transfer of Petrobacter succinatimandens to the genus Tepidiphilus as Tepidiphilus succinatimandens comb. nov., emended description of the genus Tepidiphilus and

description of Tepidiphilus thermophilus sp. Nov., isolated from a terrestrial hot spring. Int. J. Syst. Evol. Microbiol. 64, 228–235. https://doi.org/10.1099/ijs.0.056424-0.

Revie, R.W., Uhlig, H.H., 2008. Corrosion and Corrosion Control: an Introduction to Corrosion Science and Engineering, first ed. Wiley. https://doi.org/10.1002/9780470277270.

Örnek, D., Jayaraman, A., Syr, B., 2002. Pitting corrosion inhibition of aluminum 2024 by bacillus biofilms secreting polyaspartate or γ-polyglutamate. Appl. Microbiol. Biotechnol. 58, 651–657. https://doi.org/10.1007/s00253-002-0942-7.

Rutala, W.A., 2008. Guideline for Disinfection and Sterilization in Healthcare Facilities, vol 2008.

Schmitt, F.-J., Renger, G., Friedrich, T., Kreslavski, V.D., Zharmukhamedov, S.K., Los, D. A., Kuznetsov, V.V., Allakhverdiev, S.I., 2014. Reactive oxygen species: Re-evaluation of generation, monitoring and role in stress-signaling in phototrophic organisms. Biochim. Biophys. Acta Bioenerg. 1837, 835–848. https://doi.org/10.1016/j.bbabio.2014.02.005.

Scott, D.A., 1990. Bronze disease: a review of some chemical problems and the role of relative humidity. J. Am. Inst. Conserv. 29, 193–206. https://doi.org/10.1179/019713690806046064.

Setlow, P., 2006. Spores of bacillus subtilis: their resistance to and killing by radiation, heat and chemicals. J. Appl. Microbiol. 101, 514–525. https://doi.org/10.1111/j.1365-2672.2005.02736.x.

Singh, V.B., Singh, R.N., 1995. Corrosion and inhibition studies of copper in aqueous solutions of formic acid and acetic acid. Corros. Sci. 37, 1399–1410. https://doi.org/10.1016/0010-938X(95)00042-I.

Solioz, M., Abicht, H.K., Mermod, M., Mancini, S., 2010. Response of Gram-positive bacteria to copper stress. J. Biol. Inorg. Chem. 15, 3–14. https://doi.org/10.1007/s00775-009-0588-3.

Tait, W.S., 2018. Electrochemical corrosion basics. In: Handbook of Environmental Degradation of Materials. Elsevier, pp. 97–115. https://doi.org/10.1016/B978-0-323-52472-8.00005-8.

Videla, H.A., 2018. Manual of Biocorrosion, first ed. Routledge. https://doi.org/10.1201/9780203748190.

Vivier, V., Orazem, M.E., 2022. Impedance analysis of electrochemical systems. Chem. Rev. 122, 11131–11168. https://doi.org/10.1021/acs.chemrev.1c00876.

White, R.H., 1984. Hydrolytic stability of biomolecules at high temperatures and its implication for life at 250 °C. Nature 310, 430–432. https://doi.org/10.1038/310430a0.

Yu, J., Huang, X., Ren, F., Cao, H., Yuan, M., Ye, T., Xu, F., 2024. Application of antimicrobial properties of copper. Appl. Organomet. Chem. 38, e7506. https://doi.org/10.1002/aoc.7506.

Özdemir, S., Kılınç, E., Poli, A., Nicolaus, B., 2013. Biosorption of Heavy Metals (Cd^{2+}, Cu^{2+}, Co^{2+}, and Mn^{2+}) by Thermophilic Bacteria, *Geobacillus thermantarcticus* and *Anoxybacillus amylolyticus* : equilibrium and Kinetic Studies. Biorem. J. 17, 86–96. https://doi.org/10.1080/10889868.2012.751961.

Zhang, X., Wang, G., Ma, X., Yu, J., You, J., Xue, Y., Ma, Y., 2020. Tepidiphilus baoligensis sp. Nov., a novel bacterium of the family Hydrogenophilaceae isolated from an oil reservoir. Curr. Microbiol. 77, 1939–1944. https://doi.org/10.1007/s00284-020-01983-8.

Zhang, Y., Xiang, Y., Yang, Z., Xu, R., 2024. Co-occurrence of dominant bacteria and methanogenic archaea and their metabolic traits in a thermophilic anaerobic digester. Environ. Sci. Pollut. Res. 31, 36716–36727. https://doi.org/10.1007/s11356-024-33699-8.

Zhe, Y., Pehkonen, S.O., 2004. Copper corrosion kinetics and mechanisms in the presence of chlorine and orthophosphate. Water Sci. Technol. 49, 73–81. https://doi.org/10.2166/wst.2004.0092.